ASSEMBLY, VERIFICATION, INTEGRATION AND TESTING OF THE PAYLOAD AND COMMUNICATIONS SYSTEM OF THE 3CAT-4 CUBESAT

A Degree Thesis

Submitted to the Faculty of the

Escola Tècnica d'Enginyeria de Telecomunicació de Barcelona

Universitat Politècnica de Catalunya

by

Amadeu Gonga Siles

In partial fulfilment

of the requirements for the degree in

TELECOMMUNICATIONS SYSTEMS ENGINEERING

Advisor: Prof. Adriano José Camps Carmona

Ms. Lara Fernández Capón

Barcelona, September 2020

Abstract

Since their standardization around 2000, nanosatellites have experienced an enormous growth.

The UPC-NanoSat Lab, located in Campus Nord of the Universitat Politècnica de Catalunya, aims to explore and develop innovative applications and remote sensing techniques for nanosatellites always focusing on students teaching allowing them to conceive, design, implement, test and operate the subsystems that conforms a CubeSat.

^{3}CAT-4 project, supported by European Space Agency (ESA) 'Fly Your Satellite!' programme, is planned to be finished and ready to launch in spring of 2021 with the implementation of three experiments for Earth observation: an L-band Microwave Radiometer, a GNSS (Global Navigation Satellite Systems) Reflectometer, and an AIS (Automatic Identification System) receiver.

During the time lapse of this thesis, it has been performed the verification of the L-band Microwave Radiometry experiment at ambient temperature and at adverse temperatures apart from the communications subsystem (COMMS) verification at ambient temperature.

Resum

Els nanosatèl·lits han experimentat un important creixement en aquests darrers anys des de que van ser estandarditzats al 2000.

El UPC-NanoSat Lab, que es troba al Campus Nord de la Universitat Politècnica de Catalunya, pretén explorar i desenvolupar aplicacions innovadores i tècniques de teledetecció per a nanosatèl·lits sempre des del punt de vista d'ensenyament pels estudiants permetent-los concebre, dissenyar, implementar, testejar i operar els subsistemes que conformen un CubeSat.

El projecte ^{3}CAT-4, recolzat pel programa 'Fly Your Satellite!' de l'Agència Europea de l'Espai (ESA), està previst que sigui finalitzat i llest pel seu llançament a l'estiu del 2021 amb la implementació de tres experiments per a l'observació de la Terra: un Radiòmetre de microones a la banda L, un reflectòmetre de senyals GNSS (Sistema Global de Navegació per Satèl·lit), i un receptor AIS (Sistema d'Identificació Automàtic).

Durant el lapse temporal d'aquesta tesis, s'ha dut a terme la verificació del radiòmetre de microones a temperatura ambient i en temperatures adverses a part de la verificació del subsistema de comunicacions (COMMS) a temperatura ambient.

Resumen

Los nanosatélites han experimentado un importante crecimiento en estos últimos años desde que fueron estandarizados en 2000.

El UPC-NanoSat Lab, que se encuentra en el Campus Nord de la Universidad Politécnica de Cataluña, pretende explorar y desarrollar aplicaciones innovadoras y técnicas de teledetección para nanosatélites siempre desde el punto de vista del aprendizaje para los estudiantes permitiéndoles concebir, diseñar, implementar, testear y operar los subsistemas que conforman un CubeSat.

El proyecto ^{3}CAT-4, apoyado por el programa 'Fly Your Satellite!' de la Agencia Europea del Espacio (ESA), está previsto que finalice y sea lanzado el verano de 2021 con la implementación de tres experimentos para la observación de la Tierra: un Radiómetro de microondas en banda L, un reflectómetro de señales GNSS (Sistema Global de Navegación por Satélite), y un receptor AIS (Sistema de Identificación Automático).

Durante el lapso temporal de esta tesis, se ha llevado a cabo la verificación del radiómetro de microondas a temperatura ambiente y en temperaturas adversas a parte de la verificación del subsistema de comunicaciones (COMMS) a temperatura ambiente.

Acknowledgements

I would like to express my gratitude to Prof. Adriano Camps (project supervisor) and all the NanoSat Lab staff, in special to ^{3}CAT-4 project leader and co-supervisor Lara Fernández, hardware engineer Marc Badia, and technician Albert Martón for their gratitude and helpfulness towards me making the development of the thesis easier.

On the other hand, I would like to thanks to European Space Agency for giving the opportunity to ETSETB students to form part of their CubeSats educational programme allowing them to introduce and learn about the world of satellites.

Revision history and approval record

Revision	Date	Purpose
0	30/06/2020	Document creation
1	16/08/2020	Document revision
2	20/08/2020	Document closure

DOCUMENT DISTRIBUTION LIST

Name	e-mail
Amadeu Gonga Siles	agongasiles@hotmil.com
Adriano José Camps Carmona	camps@tsc.upc.edu
Lara Pilar Fernández Capón	lara-pilar.fernandez@tsc.upc.edu

Written by: Amadeu Gonga		Reviewed and approved by: Adriano Camps	
Date	14/08/2020	Date	16/08/2020
Position	Project Author	Position	Project Supervisor

Table of contents

List of Figures

List of Tables

1. Introduction

^{3}Cat-4 (read as “cube-cat-four”) is the fourth member of the CubeSat series of UPC’s NanoSat Lab. [1]

The project was selected by European Space Agency (ESA) in 2017 as part of the 2nd ‘Fly Your Satellite!’ programme giving UPC students the possibility to work in a CubeSat project with ESA supervision in the design, development and validation of a 1U CubeSat (100 x 100 x 113.5 mm^{3}) and its GS (Ground Station).

^{3}Cat-4 mission is focused on evaluating L-band Microwave Radiometry, GNSS-R, and AIS receiver all of them hosted in a payload.

Regarding to the physical architecture of the ^{3}Cat-4, this is composed by different subsystems:

- ZADS (Zenith Antenna Deployment System): monopole deployable antenna system which contains VHF and UHF antennas.
- AOCS&COMMS (Attitude and Orbit Control System & Communications): module responsible of the determination and control of the spacecraft orientation as well of its communications between the GS and itself.
- OBC&IB (On Board Computer & Interface Board): subsystem which provides the capability of processing and interfacing with the other subsystems as well of connecting the satellite to the PC for programming and debugging.
- EPS (Electrical Power Supply): it has the function to gather, collect and provide the necessary electrical power.
- FMP (Flexible Microwave Payload): it is the spacecraft’s payload integrating the three mission experiments in a single hardware platform.
- NADS (Nadir Antenna Deployment System): contains the L-band antenna for the FMP data acquisition and the Gravity Boom to generate Gravity Gradient.
- SP (Solar Panels): module responsible to collect the solar energy and to determine the satellite orientation using Sun sensors.

Figure 1 shows a ^{3}CAT-4 render to give a better idea about how are stacked each subsystem inside the spacecraft structure.

In this thesis the reader can find the verification performed to the L-band Microwave Radiometry experiment which is constituted by a TPR (Total Power Radiometer) distributed between the FMP and NADS subsystems.

Moreover, it can be found the environmental testing performed over the TPR once it is verified at ambient temperature in order to simulate the temperatures that will cope with once in space discarding any undesired behaviour while operating.

On the other hand, it can be find the verification of COMMS subsystem by retrieving and transmitting some telemetry commands.

In Appendix A can be found the work plan and a Gantt chart of the project describing all the work packages and delays that had arisen during this project.

2. State of the art of the technology used or applied in this thesis:

Sputnik-1 and -2, Explorer-1 and Vanguard-1 were the first four artificial Earth satellites launched by humans. Except Vanguard-1, the satellites Sputnik-1 and -2 and Explorer-1 did not have solar panels so their mission ended after few weeks when batteries died.

Sputnik-1 was launched in 1957 into a LEO (Low Earth Orbit) weighing approximately 84 kg being a metal sphere of 58 cm.

During the first two decades of the space age, each satellite had its own design. In the early 80's, micro-satellites emerged and adopted a radically different design to reduce costs, focusing on available and existing technologies, and using properly qualified COTS (Commercial Off-The-Shelf) components.

2.1. The CubeSat Standard

In 1999, Professors Jordi Puig-Suari and Bob Twiggs from California Polytechnic State University and Stanford University respectively, conceived the so-called "CubeSat standard" allowing graduate students to conceive, design, implement, test and operate in space a complete spacecraft in a "reasonable" amount of time.

CubeSats are small satellites multiples of 1U (1U: 10 x 10 x 11.35 cm^3, weighing less than 1.33 kg) that include all the basic subsystems as in large satellites but using COTS components.

The main application of CubeSats nowadays is the Earth Observation (EO) field thanks to the intense R&D performed in the three most challenging difficulties that they have. On one side, due to their small size it has been difficult to include deployable solar panels. On the other side, it has been difficult to include large antenna reflectors and to transmit enough RF power so as to have a satisfactory space-to-Earth link budget. The third challenging aspect was the pointing accuracy that now has significantly improved thanks to miniaturized star-trackers and reaction wheels.

2.2. Most Pioneer Organizations in CubeSats

Until 2013 most of the CubeSats were launched by Universities and research institutes, and most of them were 1U or 2U. However, in 2013 the first 3U CubeSat from Planet Labs Inc. and Spire Global Inc. were launched. From then until 2019, these two companies had launched the largest commercial constellations with 355 and 103 CubeSats respectively.

It took about a decade to NASA (National Aeronautics and Space Administration) since the CubeSat standard emerged to start the Educational Launch of Nanosatellites (ELaNa) in 2010 [2]. This fact provided NASA opportunities to test and validate new science instruments in CubeSats to advance its science portfolio.

On the other hand, ESA launched in February 2008 the first call to universities for CubeSat proposals and seven of them were launched in February 2012. Since then, 12 more CubeSats have been enrolled in the first and second editions of the "Fly Your Satellite!" programme, ^{3}CAT-4 among them.

2.3. Way Forward

With their standardization in 1999, CubeSats have grown from simple educational applications to eventually displacing medium size competing satellites. However, CubeSats cannot displace all the large missions as physics laws cannot be changed, i.e. large apertures and focal lengths are required to collect faint signals and achieve large angular resolution.

As mentioned before, their main applications are in EO, but Astronomy and Communications applications are emerging thanks to the short revisit times or the continuous monitoring using constellations of CubeSats.

Early CubeSats had short lifetimes once in orbit (a few months), but by testing and adding redundancies, lifetimes have grown up to 4-5 years in some cases.

Despite all these improvements, in order to exploit the full potential of CubeSats, many technologies still need to be developed such as communications performance, reliability, thermal stability, calibration accuracy, among others.

The interested reader is encourage to consult [3] for more detailed information.

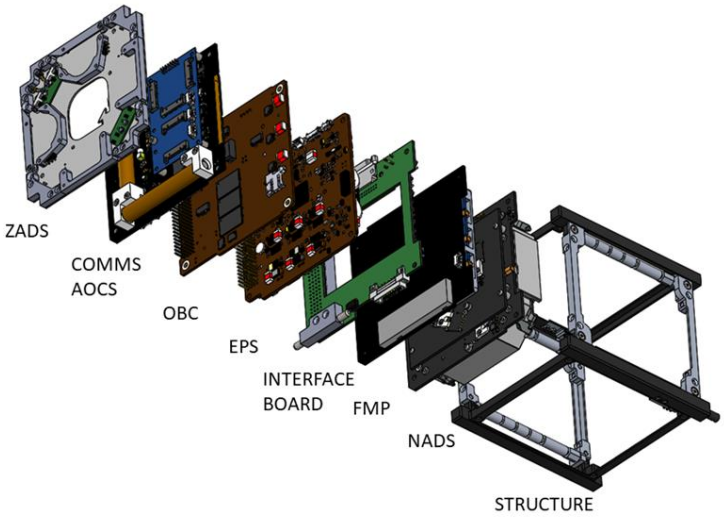

Figure 1: [3]CAT-4 spacecraft decomposition [1]

2.4. Microwave Radiometry in CubeSats

Microwave radiometry is the science of the measurement of the noise emitted by bodies at a physical temperature higher than zero Kelvin.

This principle begins with Kirchhoff's law which states that for all materials at a thermodynamic equilibrium, all the absorbed power must be reradiated, otherwise, if they radiate more power than their absorb, their physical temperature would decrease indefinitely and vice versa, if they absorb more power than they emit, their physical temperature would increase indefinitely.

It can be demonstrated that the power received by an antenna from the bodies' emission can be defined as (1), and it depends on the so-called antenna's temperature (T_A), and receiver's noise bandwidth (B). The other parameter refers to Boltzmann's constant (k_B).

$$P \triangleq k_B \cdot T_A \cdot B \tag{1}$$

CubeSats use this science in the field of EO since they are capable of measuring the Earth's surface temperature from space in a limited frequency bandwidth. This fact turns into a higher level of complexity in the microwave radiometry because there are many more aspects to take into account in this scenario like the atmospheric, rain, cloud, fog attenuations, or the polarization rotation in the ionosphere due to the interaction between the electromagnetic wave and the magnetic field of the Earth. Moreover, depending on the type of soil (bare soil, vegetated soil or snow-covered soil) the behaviour of the emission varies. The same occurs with the ocean emission which depends on the roughness of the surface, the level of salinity, if there are oil spills from vessels or if there is ice in the sea surface.

There are several different types of real aperture radiometers but the one equipped in [3]CAT-4 is the TPR. This one has an antenna that collects the radiation in a given band, which is amplified and filtered since the power level at its input is very low. Finally, there is a power detector and average (low-pass filtered) that provides a voltage on its output.

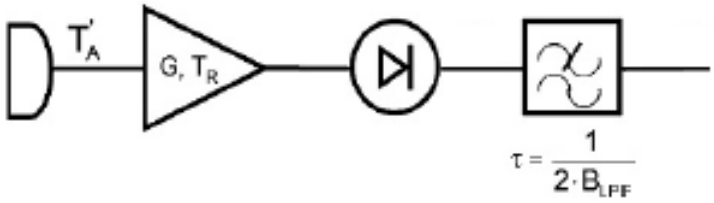

Figure 2: TPR basic block diagram [4]

To sum up, the TPR is the one in charge to deliver a voltage on its output approximately linear with its input power, proceeding from the bodies' radiation.

Furthermore, microwaves radiometers require to be calibrated periodically. Radiometer calibration refers to the process of finding the relationship between the radiometer's output (V_d) and the input antenna temperature (T_A), by means of well-known internal or external targets (Figure 3).

$$V_d = \frac{1}{a}(T_A - b) \tag{2}$$

$$T_A = a \cdot V_d + b \tag{3}$$

In the case of [3]CAT-4, two internal calibration targets are used. One target is the cold load and it is characterized by a LNA (Low-Noise Amplifier) connected backwards delivering a low power or temperature. The second target is the hot load and it is characterized by a ML (Matched Load) delivering a higher value of power respect the cold load. Calculating the slope (a), and the ordinate at the origin (b), the transfer function is fully characterized.

Only two targets are used when considering the radiometer's response linear, otherwise additional input known temperatures would be required to determine the non-linear transfer function.

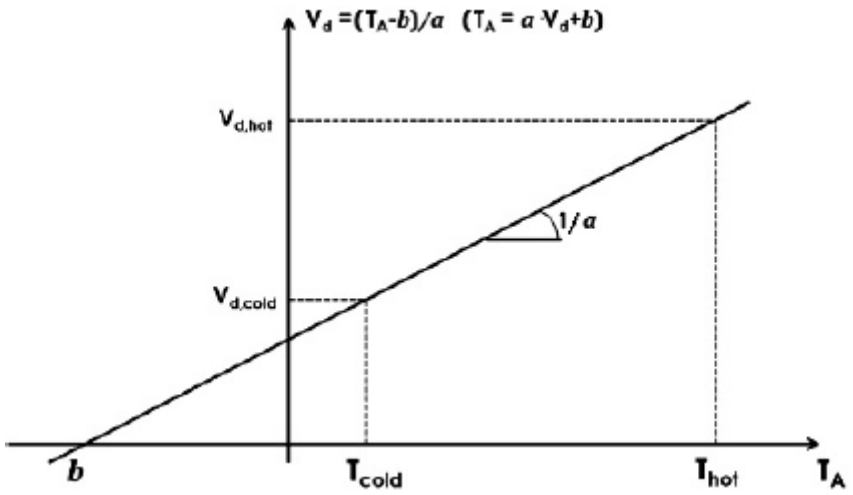

Figure 3: Radiometer calibration plotting the linear response between the temperature vs. the output voltage [4]

Radiometric precision refers to how deviated from the real temperature emitted by bodies is the temperature captured and delivered by the radiometer.

Ideally, the radiometric precision from the TPR is given by:

$$\Delta T = \frac{T_{sys}}{\sqrt{B \cdot \tau}} \tag{4}$$

where $T_{sys} = T_R + T_A$ and τ it is the integration time. Note that by increasing the receiver's bandwidth and/or the integration time, radiometric precision improves.

However, expression (4) is ideal in the sense that it does not take into account any receiver imperfections except for the thermal noise. The main limitations of the TPRs come from the gain fluctuations of the receiver chain (Tiuri, 1964 [5]) generating thermal drifts attributed to a variation of the antenna temperature generating a variation of the measured system's temperature.

$$\Delta T = T_{sys}\left[\frac{1}{B \cdot \tau} + \left(\frac{\Delta G_s}{G_s}\right)^2\right]^{\frac{1}{2}} \tag{5}$$

It should be guaranteed that those gain fluctuations ($\frac{\Delta G_s}{G_s}$) are not larger than $\frac{1}{B \cdot \tau}$ otherwise the measured system's temperature would be polluted by them providing a wrong value of the temperature.

The interested reader it is invited to visit the book published by the project supervisor of this thesis with very useful information about satellites remote sensing where it can be found in more detail the science of microwave radiometry. [4]

3. Methodology / project development:

3.1. Model Philosophy

^{3}CAT-4 mission is based on a Protoflight Model (PFM) philosophy. This means that only one spacecraft is built, and qualified for flight which is the PFM or sometimes referred as Flight Model (FM).

Nevertheless, PFM is not the only model built, Qualification Model (QM) and Engineering Model (EM) are also models used for different purposes.

3.1.1. Protoflight Model

This can be the spacecraft built and qualified for flight, or the subsystems used to assemble the PFM spacecraft. During all the AIV (Assembly Integration and Verification) phases, spacecraft and subsystems PFM must be handled with extreme care inside a Cleanroom ISO 8 class or less.

The test level that PFMs must successfully pass is the qualification level while the test duration must be acceptance.

3.1.2. Qualification Model

All the subsystems developed in NanoSat Lab have several QMs used for the CDR (Critical Design Review) validation or further tests. They are very exact replicas of the PFM without conformal coating which is a thin polymeric film used to protect the PCB components in space.

QM does not have any handling restrictions so they do not need to be manipulated inside a Cleanroom.

The test level that QMs must successfully pass is the qualification level as well for the test duration.

3.1.3. Engineering Model

This model is manufactured according to the CDR design but without being validated neither being exact replicas of any QM or PFM.

The purpose of EM is to serve as a development tool, either for software and/or hardware, and to help to prepare the tests and ground support equipment. Therefore, they do not represent the performance of QMs and PFMs, and are not subject to any handling restrictions.

3.2. Subsystem Development Process

The first step before proceeding with the assembly of any subsystem consists of the preparation of all the components needed as well of the PCB. The PCB receives a bake-out in order to remove any micro-bubbles that may have appeared between the PCB and the solder mask during its manufacturing. The reason is to avoid that these micro-bubbles do not exploit in space due to pressure causing damages in the subsystems.

Once all the components are available and the PCB is baked-out, the next step is the assembly of the components into the PCB following the AIProc (Assembly and Integration Procedure) document where there are defined all the steps to perform in order to successfully carry out the assembly.

Next step once the subsystem is assembled consists in the Standalone Subsystem Verification (SSV) at ambient temperature. All the tests that a subsystem needs to perform are previously defined and rigorously explained in a document named Test Specifications and Test Procedures (TSTP). When all the tests are done, their results are written in a last document named Test Report and Test Procedures (TRTP) where all the anomalies or deviations from the original test defined in the TSTP are exposed.

As mentioned in the Introduction, in this thesis the reader can find the verification of the TPR using PFM located between the FMP and NADS subsystems and the verification of COMMS PFM subsystem.

After the SSV at ambient temperature, following the same structure with the documentation as mentioned before, takes place the ETC (Environmental Test Campaign) where the subsystems are tested and verified under the most probably extreme temperatures that each of them will face at space under vacuum conditions.

Also in this thesis the reader can find the ETC performed over the TPR PFM.

When the verification of a subsystem at ambient temperature and at adverse temperatures is successfully done, the subsystem is integrated in the FlatSat where all the subsystems instead of being stacked like in the CubeSat structure (Figure 1), they are integrated side by side. The reason of this configuration is because it is easier to carry out a full functional test having all the subsystem together connected.

The last step once all the spacecraft subsystems work correctly would be the integration inside the CubeSat structure for future tests performed over the whole spacecraft since this will be the one launched to the space.

4. Results

In this sections the reader can find a brief description about how are composed the TPR experiment and COMMS subsystem and also their verification either at ambient temperature or during an ETC in the case of the TPR.

4.1. TPR Verification

Microwave radiometry is one of the three mission experiments aboard [3]CAT-4. This is hosted between two subsystems, NADS Antenna Bottom PCB and FMP.

The TPR is designed to work at L-band, more specifically between $f_1 = 1400$ MHz and $f_2 = 1427$ MHz, because it is the reserved band in the frequency spectrum with the largest sensitivity to soil moisture and ocean salinity, and at this band the attenuation presented by the atmosphere is almost negligible.

In the following subsections, the reader can find the TPR E2E (end-to-end) behaviour for a first NADS Antenna Bottom version exhibiting its main problems detected during its debugging and how those problems were attacked and solved in a second version.

4.1.1. FMP + NADS Antenna Bottom V1.0

4.1.1.1. Block Diagram

First version applied for the TPR is shown in Figure 4, in which NADS Antenna Bottom is composed by the calibration loads, a LNA, and a switch that is the one in charge about commuting between the L-band helix antenna and the calibration loads.

Then, the RF signal is lead to the FMP where there are hosted the other experiments. First to notice is that in the FMP, a first switch routes the path coming from the NADS Antenna Bottom into three. The reason of this is because the GNSS down-looking experiment is in the same RF L-band like the TPR, meaning that several blocks are shared between both experiments as well the L-band helix antenna.

It is not until the second FMP's switch that the AIS, GNSS and L-band Radiometer experiments are grouped and processed by the SDR which is the digital unit of the RF receiver that performs demodulations and additional operations.

Note that the topology used in [3]CAT-4 limits the payload subsystem in terms of operation letting the execution of each experiment sequentially on time since there is only one receiver.

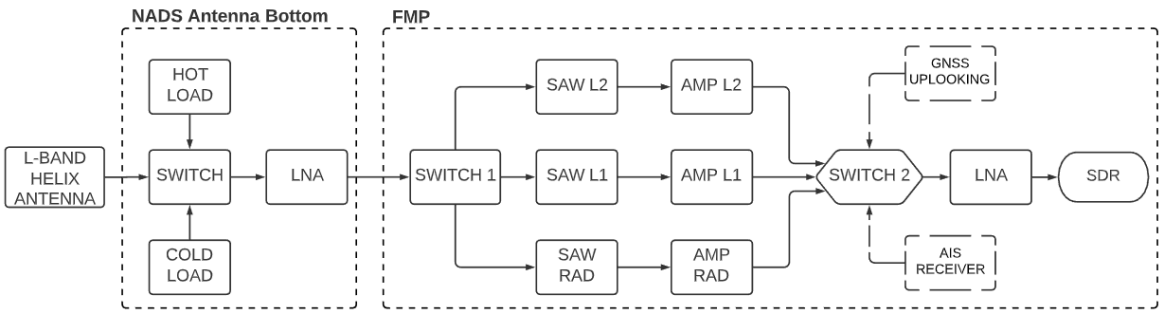

Figure 4: TPR block diagram V1.0

4.1.1.2. Performance at Ambient Temperature

The reason because there are two NADS Antenna Bottom versions is because of the wrong performance of the first one due to four main reasons encountered during the first tests. Before explaining those reasons, Figure 5 shows the noise power collected by the spectrum analyzer at the FMP's output when activating the HL (Hot Load), Figure 6 corresponds to the noise power when the ACL (Active Cold Load [6]) is activated, and Figure 7 when the antenna is activated having a ML (Matched Load) at its input. Theoretically, Figure 5 and Figure 7 should have the same spectral response since in the antenna's input it was placed a ML meanwhile the HL consists in a ML as well.

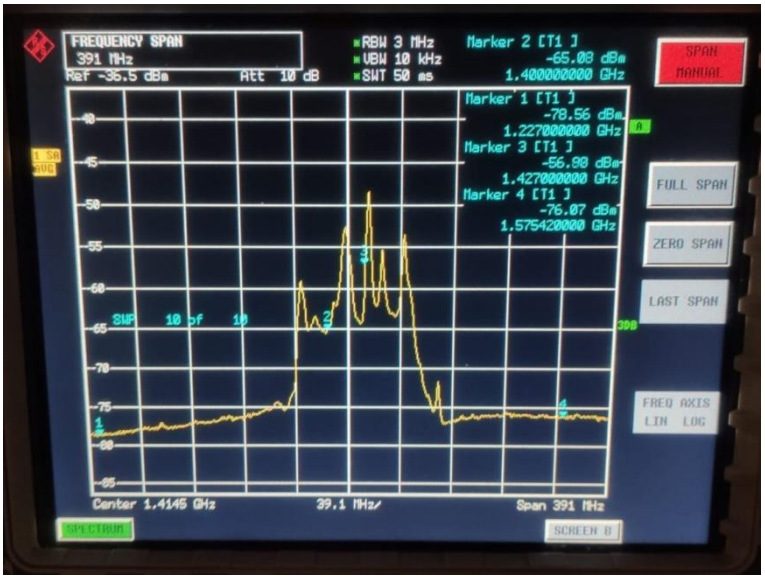

Figure 5: HL spectrum response V1.0

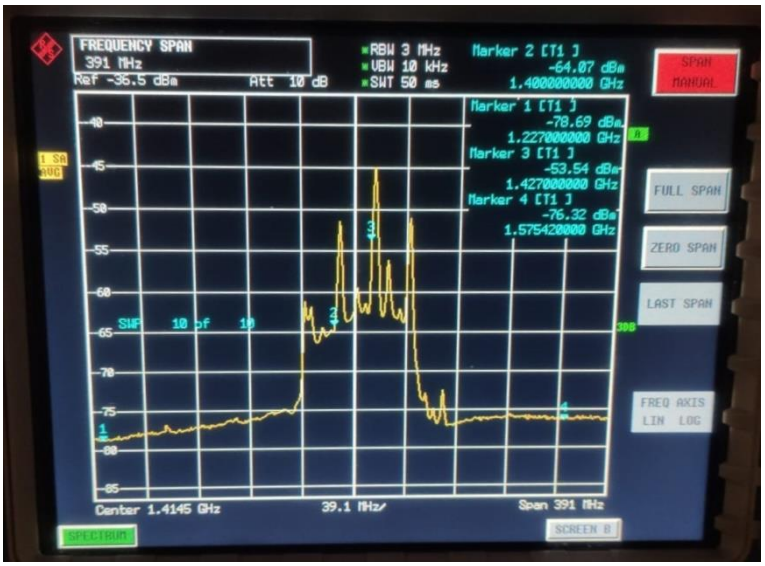

Figure 6: ACL spectrum response V1.0

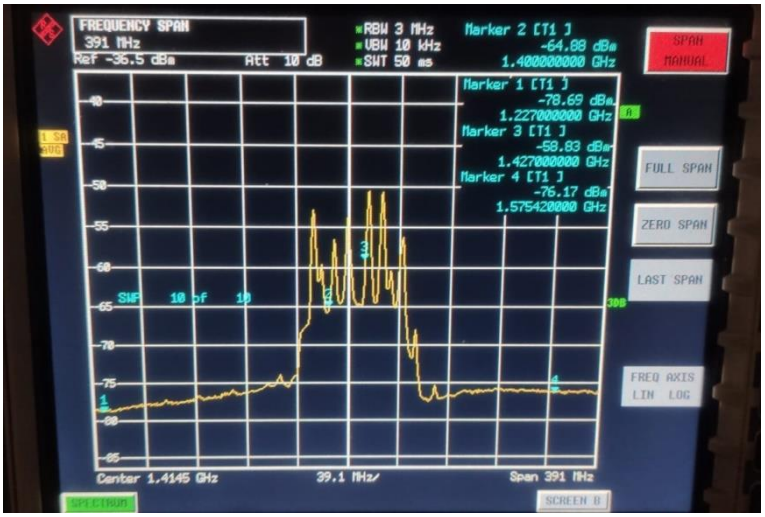

Figure 7: Antenna spectrum response V1.0 (with a ML at its input)

The reader will quickly notice that in the pass band there were signal peaks or spurious signals polluting the response that the HL, ACL or antenna should have. Moreover, the power level between the HL and the ACL (without taking into account the peaks) do not vary much, it is practically the same, and this is not correct.

Knowing that the TPR response for the NADS Antenna Bottom V1.0 it is not the desired one, there is no choice, but to start debugging the circuit layout in order to figure out the responsible of its incorrect performance.

The first anomaly found was the LNA matching circuit [13]. Some active components like LNA need to have different configurations of passive components like resistors, capacitors or inductors at its input and output in order to guarantee the performance in which they are made for. This configuration is defined in their datasheet specifying the components and values needed depending on the working frequency.

In the NADS Antenna Bottom V1.0, the matching circuit shown in Figure 8 the capacitor C5 at its input was missing, and the value of L4 was not the specified one, but a different one. Due to this fact, the LNA could not have been working in a stable region producing an undesired performance (oscillations).

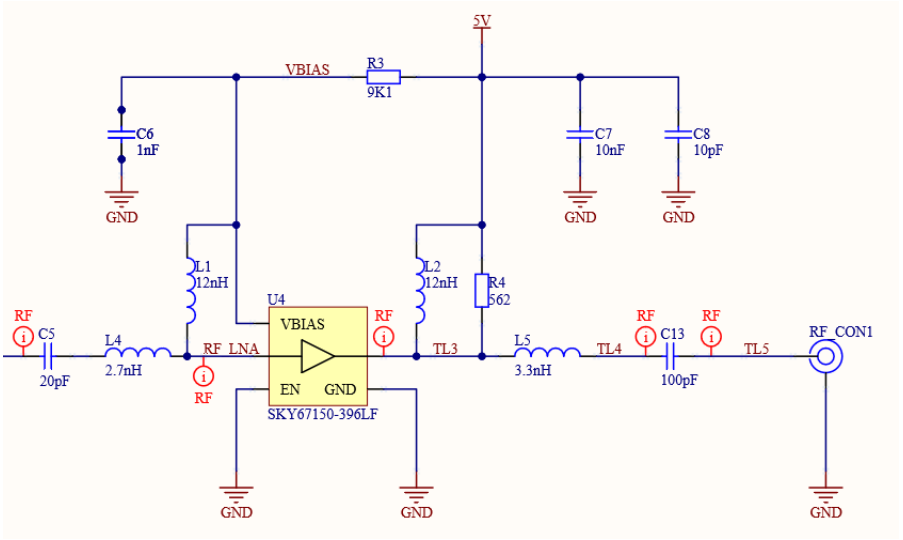

Figure 8: LNA schematic with its adaptation circuit

The second anomaly found was the wrong width of the RF lines which mainly depends on the characteristic impedance, the frequency, the dielectric constant, the conductor thickness and height. This fact is translated into a characteristic impedance of the RF lines different from 50 Ω creating additional signal mismatches. This error was solved in the NADS Antenna Bottom V2.0 layout even though this anomaly should not be related with the incorrect performance of the TPR.

The third anomaly found was related to the NADS Antenna Bottom supply voltage. NADS Antenna Bottom has a 6 pin PicoBlade proceeding from the FMP, 2 pins for the switch control voltage, one pin for the temperature sensor voltage reading, one GND and the last ones for the 5 V and 3.3 V were missing.

It was realized that depending on the position of the 6 wires, the signal peaks seen in the spectrum analyzer before were attenuated or amplified meaning that the voltage coming from the FMP could be polluted by some sort of EMI (Electromagnetic Interference). In order to see the stabilization of the 5 V and 3.3 V voltages, they were analysed in an oscilloscope measuring their AC component.

Figure 9 shows through the FFT the maximum AC amplitude that is present in the 3.3 V wire. This one is -61.2 dBV or 0.871 mV deviated from 3.3 V meaning that it is not as stable as it should be.

On the other hand, Figure 10 shows the maximum AC amplitude presence in the 5 V wire with a value of -63.2 dBV or 0.692 mV, which is not stable either.

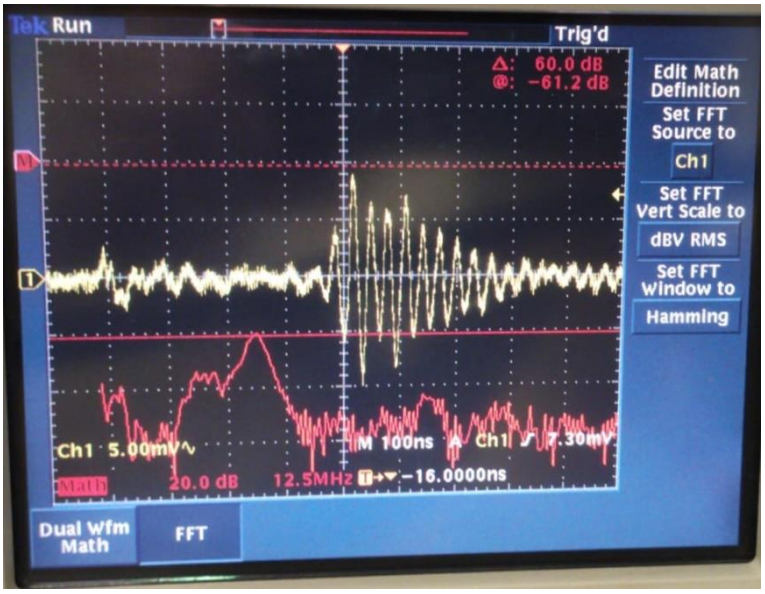

Figure 9: 3V3 wire AC ripple

As seen in section 2.4, gain fluctuations of the receiver chain generate thermal drifts attributed to the antenna temperature generating a variation of the measured system's temperature. Since the gain of a LNA may oscillate if voltage source is not stable, it is necessary to stabilize enough the voltage source to ensure a better radiometric precision [7] [8].

In order to avoid this problem, the solution remains in placing LDOs at the 5 V and 3.3 V lines for its stabilization improvement (models [23] [24]). Ideally, the LDO should be placed as close as possible to the LNA voltage input but due to distribution issues, they were placed in a zone where they fit in NADS Antenna Bottom V2.0.

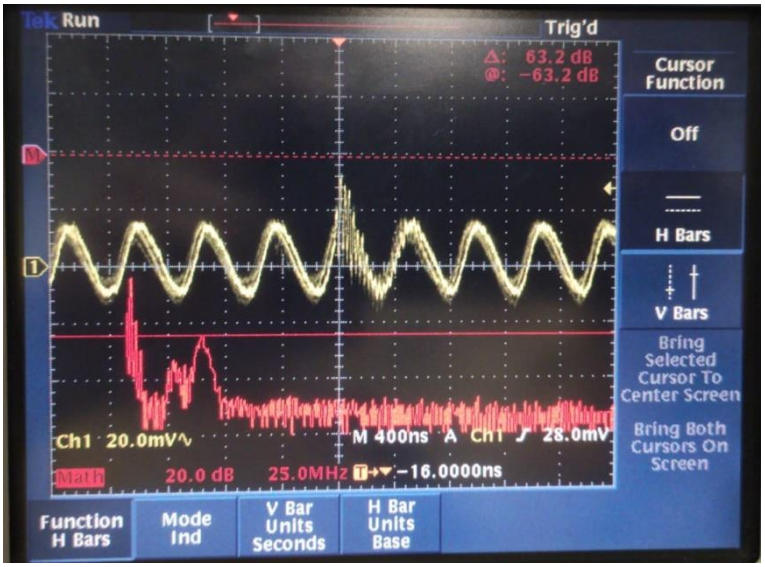

Figure 10: 5V wire AC ripple

Last anomaly found was related with the SMA connector placed at the L-band helix antenna's input in order to inject and simulate a signal that could have been received by the antenna. As seen in Figure 11, the GND wire used for avoiding any grounding loop between the PCB input and output connectors, was larger enough in terms of RF that was introducing an undesired inductance. Probably this was the guiltiest anomaly of the spurious signals.

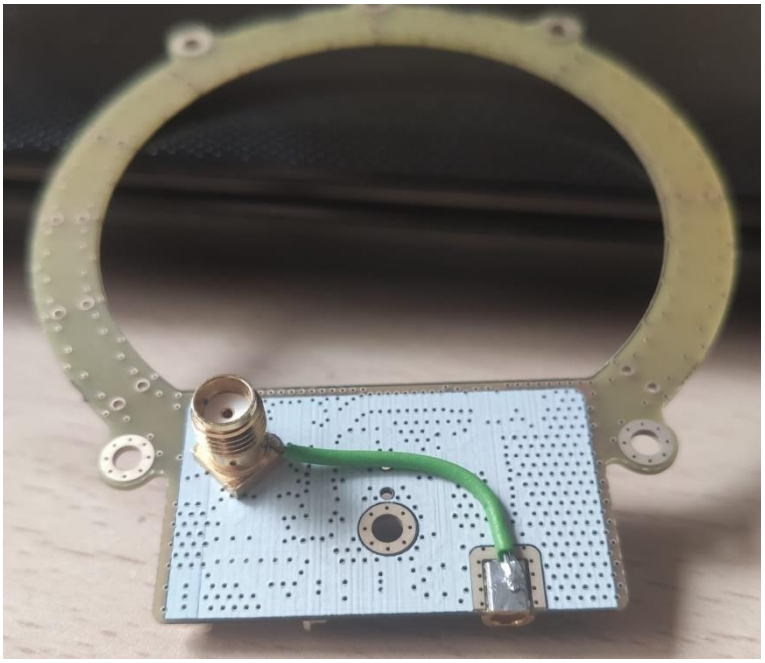

Figure 11: NADS Antenna Bottom V1.0 top view

4.1.2. FMP + NADS Antenna Bottom V2.0

4.1.2.1. Block Diagram

After the debugging performed over the NADS Antenna Bottom V1.0 achieving some anomalies that could be the reason of its bad performance, a new layout design was assembled. This one is shown in Figure 12 and basically the LNA matching circuit is fixed as well as the RF lines width. Also the LDOs are included for the improved voltage stabilization and the SMA connector has a shorter GND connection. Furthermore, the layout is tidier and includes more VIA holes for the RF signal propagation avoidance inside the NADS Antenna Bottom V2.0 PCB.

The NADS Antenna Bottom V2.0 PCB physical design is shown in Figure 13.

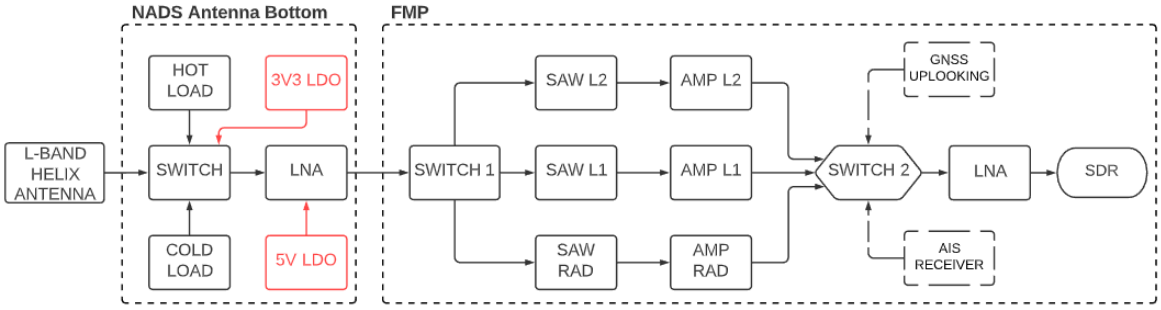

Figure 12: TPR block diagram V2.0

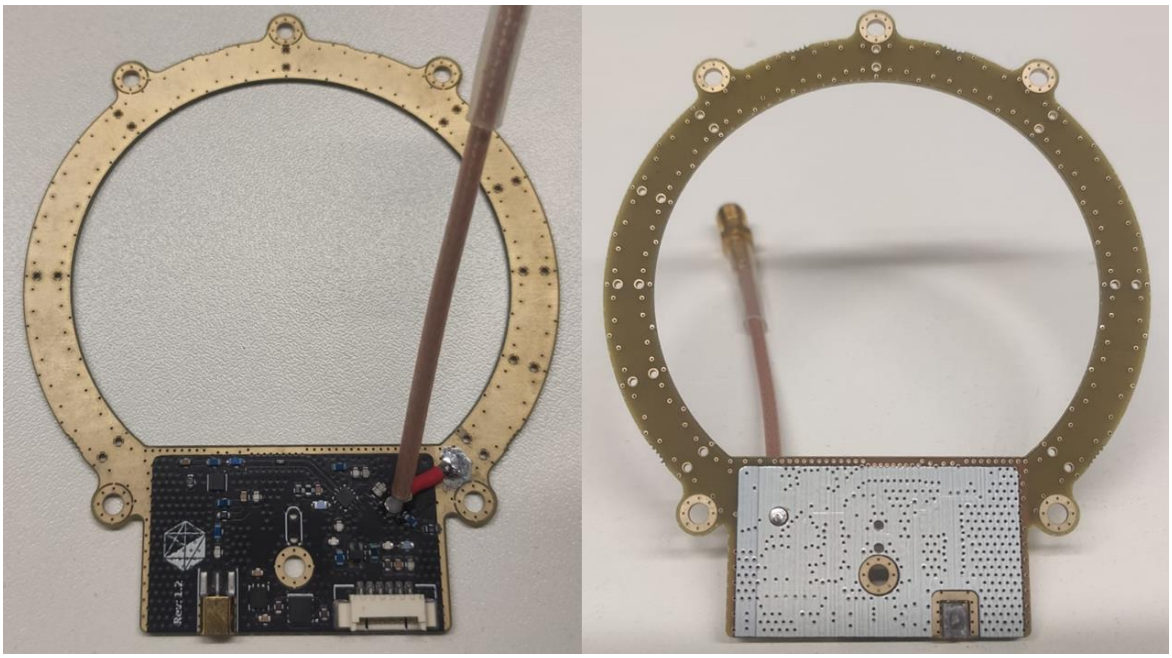

Figure 13: NADS Antenna Bottom V2.0 bottom view (left) and top view (right)

4.1.2.2. Requirements

Table 1: FMP + NADS Antenna Bottom requirements

Requirement	Description
Req. 1	The L-band radiometer shall be based on a TPR architecture.
Req. 2	The L-band radiometer shall compute the antenna's temperature of the radiometry band from $f = 1400\ MHz$ to $f = 1427$ MHz.
Req. 3	The L-band radiometer shall have a gain larger than 40 dB.
Req. 4	The TPR shall have a Noise Figure lower than 2 dB.
Req. 5	The L-band radiometer shall perform a periodic calibration with an internal cold and hot loads where the T_{cold} is between 50 and 80 K.
Req. 6	The TPR operating temperature range shall be from -5 ºC to 45 ºC.

4.1.2.3. Performance at Ambient Temperature

Once the NADS Antenna Bottom V2.0 was assembled, next step to follow consists of observing its behaviour in terms of frequency.

Figure 14 corresponds to the noise power collected by the spectrum analyzer at the FMP's output when activating the HL. Similarly, Figure 15 corresponds to the ACL and Figure 16 to the antenna having an RF signal at its input of $P_{in} = -80$ dBm centred at $f = 1.4$ GHz.

In a first view, the results obtained for the NADS Antenna Bottom V2.0 seems much coherent and interesting than the ones obtained in the V1.0 despite those signal peaks inside the pass band that later will be said from where they come from.

In order to successfully verify the TPR and be able to affirm that the results make sense, some analysis with the spectrum responses obtained will be done.

The analysis will consist of the calculation of the whole subsystem gain, its noise figure and the demonstration about the correct coherence between noise powers from the calibration loads.

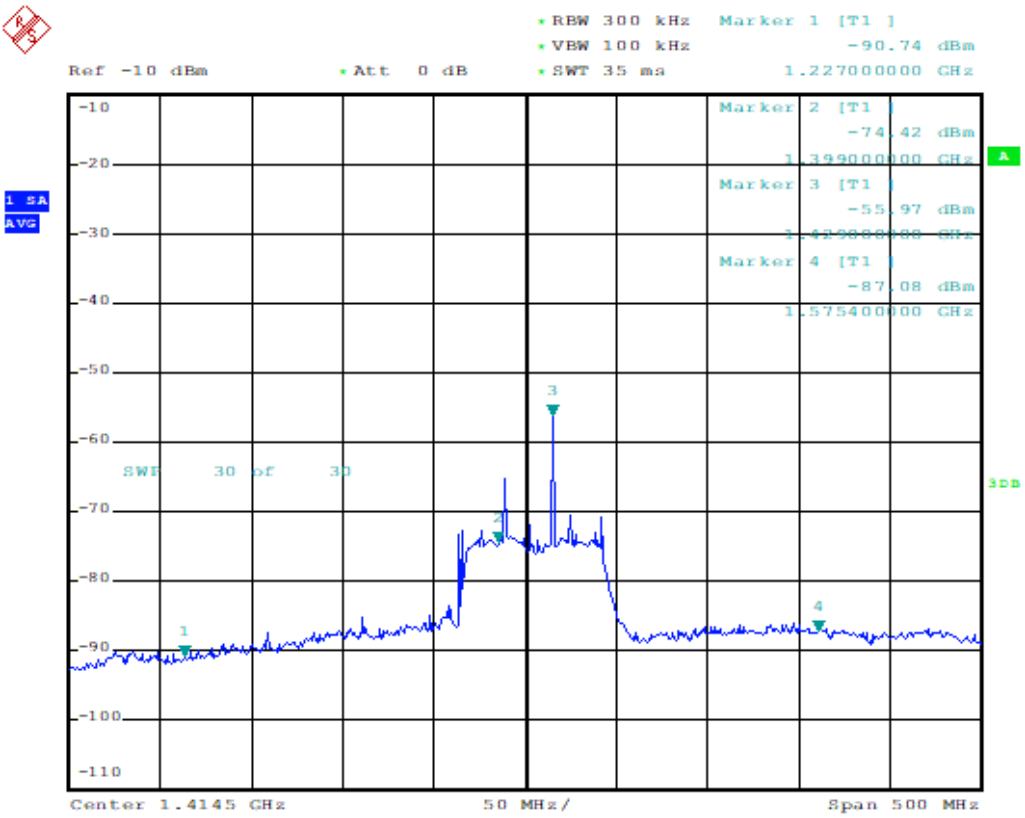

Figure 14: HL spectrum response V2.0

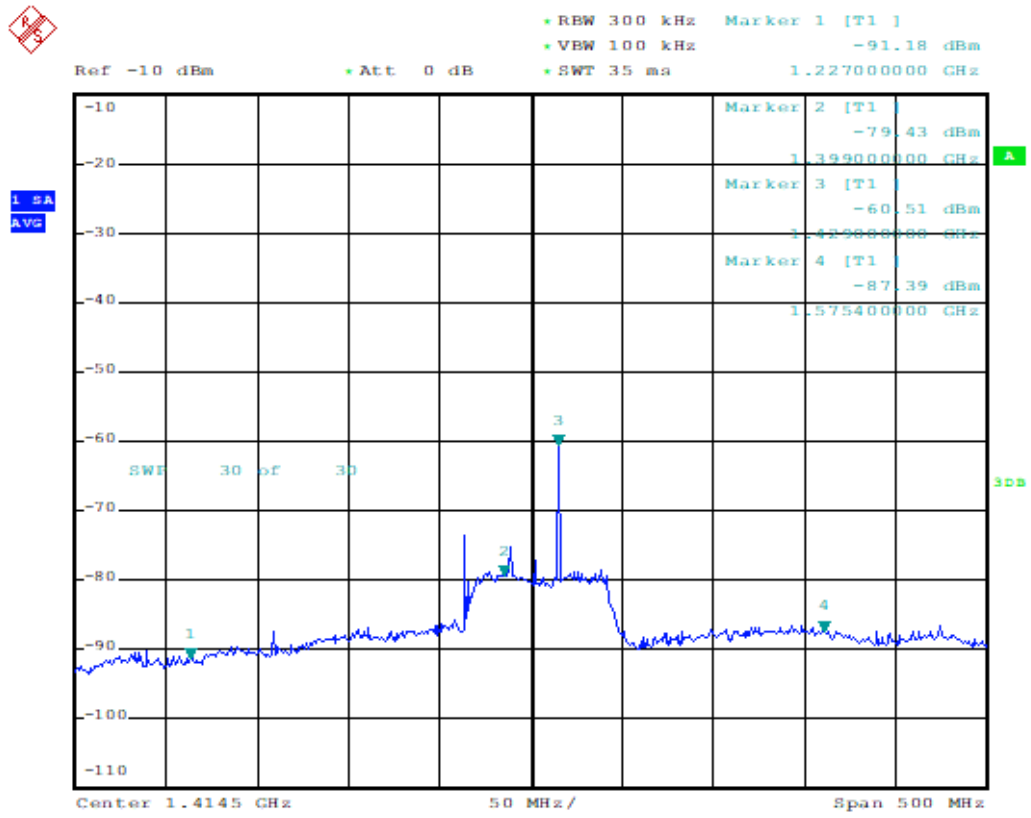

Figure 15: ACL spectrum response V2.0

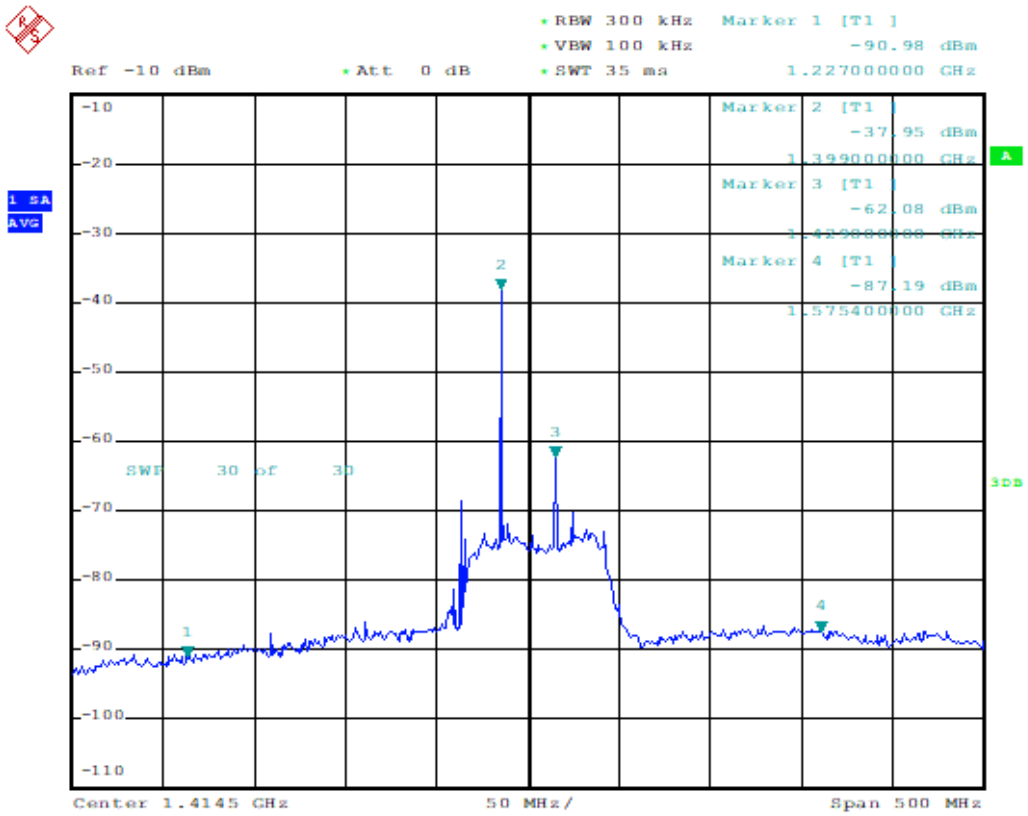

Figure 16: Antenna spectrum response V2.0 (with an input signal centred at f=1.4GHz of P_{in}=-80dBm)

a. <u>TPR Gain validation</u>

According to the component's datasheet, the whole TPR should have a gain larger than 40 dB.

The gain can be easily obtained after subtracting the power collected at the FMP's output with the one injected at the antenna's input. This will be more accurate if the losses generated by the RF wire and probe used for their connection to the spectrum analyzer are taken into account.

From Figure 16 it can be read that for an input signal of $P_{in} = -80$ dBm centred at $f =$ 1.4 GHz, this signal reaches an output power of $P_{out} = -37.95$ dBm.

Taking into account that the RF wire and probe introduce 2 dB losses, the TPR gain results:

$$G(dB) = P_{out} - (P_{in} - L) = -37.95\ dBm - (-80\ dBm - 2\ dB) = 44.05\ dB$$

Third requirement from Table 1 is fulfilled successfully.

b. TPR Noise Figure validation

The method used to determine the NF was by solving a system of equations due to the fact that there are two unknown parameters. First equation relates the receiver's output noise power (6).

$$N[dBm] = 10log_{10}\left(GkT_{sys}B\right) + 30dBm, \tag{6}$$

where:

- N is the receiver's output noise power
- G is the receiver's gain
- k is the Boltzmann's constant which is $k = 1.38 \cdot 10^{-23}$ [J·K^{-1}]
- T_{sys} is the system noise temperature and it is equivalent to $T_{sys} = T_A + T_R$ where T_A is the antenna noise temperature and T_R represents the noise generated by the receiver system.
- B is the receiver's noise bandwidth.

On the other hand, the NF is defined as:

$$NF = 10log_{10}(1 + \frac{T_R}{T_0}). \tag{7}$$

Combining equations (6) and (7), the only two parameters unknown are the NF and T_R. So, in order to obtain the NF, first it must be calculated T_R.

$$\begin{cases} N[dBm] = 10log_{10}(Gk(T_A + T_R)B) + 30dBm, \\ NF = 10log_{10}\left(1 + \frac{T_R}{T_0}\right). \end{cases} \tag{8}$$

The noise power value (N) will be the one read at the TPR's output having a ML placed at its input. Since the HL it is a ML itself, Marker 2 value from Figure 14 will be the one used for the receiver's noise power output which is $N = -74.42$ dBm. Moreover, in this situation, the antenna's temperature is the same as the ambient temperature during the test which it was approximately $T_A = 25°C = 298$ K.

Knowing that the receiver's bandwidth is limited by the spectrum analyzer resolution bandwidth (RBW) because it is the narrower filter, this is $B = RBW = 300\ kHz$.

Once all the parameters known are defined, solving the system of equation (8), T_R and NF results:

$$T_R = 10^{\frac{N-G-30}{10}} \cdot \frac{1}{kB} - T_A = 10^{\frac{-74.42-44.05-30}{10}} \cdot \frac{1}{1.38 \cdot 10^{-23} \cdot 300 \cdot 10^3} - 298 = 45.56\ \text{K}$$

$$NF = 10log_{10}\left(1 + \frac{T_R}{T_0}\right) = 10log_{10}\left(1 + \frac{45.56}{290}\right) = 0.63\ \text{dB}$$

Fourth requirement from Table 1 is fulfilled successfully.

c. Calibration loads validation

Last analysis to perform before being able to say that the TPR works properly, is related with the noise power collected from the calibration loads. In order to check if their values are correct, equation (9) provides the relationship that should be between the noise power and their temperatures. Considering known all the parameters except for T_{cold}, this one must be between 50 and 80 K to confirm that both loads work correctly.

$$\frac{T_{cold} + T_R}{T_{hot} + T_R} = \frac{P_{cold}}{P_{hot}} \tag{9}$$

First of all, the value of T_{hot} is the same as the ambient temperature during the test. This is $T_{hot} = 25°C = 298\,\text{K}$.

Secondly, it can be seen from Figure 14 that the HL noise power on average is approximately $P_{hot} = -75$ dBm and analogously from Figure 15 that the ACL noise power on average is approximately $P_{cold} = -80$ dBm.

Isolating T_{cold} from equation (9) and substituting the rest of parameters, this one results:

$$T_{cold} = \frac{P_{cold}}{P_{hot}}(T_{hot} + T_r) - T_r = \frac{10^{\frac{-80}{10}}}{10^{\frac{-75}{10}}}(298\text{K} + 45.56\text{K}) - 45.56\text{K} = 63\ \text{K}$$

Fifth requirement from Table 1 is fulfilled successfully.

Regarding to the signal peaks that can be seen in the spectrum analyzer traces, those come from the LNA that conforms the ACL since placing a probe at its output, the signal response is shown in Figure 17. Notice that the signal peaks fits with the ones at the HL, ACL or antenna spectrums but amplified. Those peaks are LNA harmonics.

The only way to reduce those harmonics would be improving the reverse isolation parameter or S_{12} of the LNA [11], but this is a parameter imposed by the component and cannot be modified. However, the solution to this problem will be the posteriori mitigation of the sampled peaks by software since between the pass band there are not much.

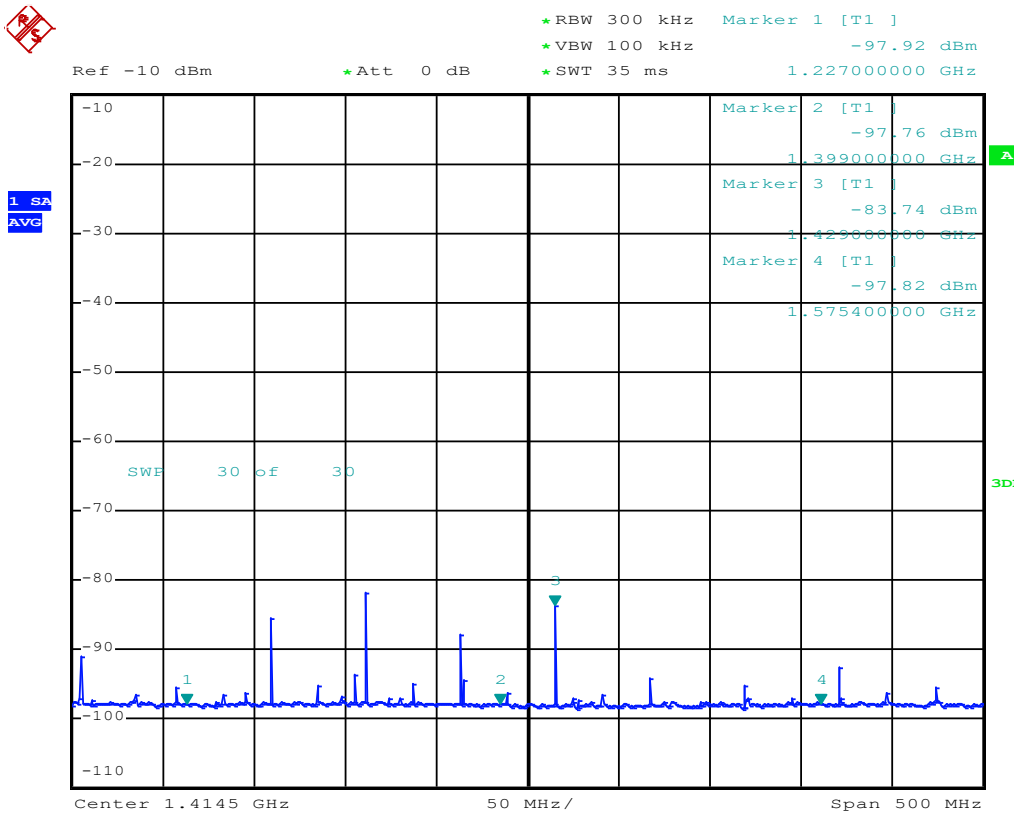

Figure 17: ACL LNA harmonics

Table 2: TPR validation summary

Parameter	Value
Current Consumption	428 mA
Noise Figure	0.63 dB
Gain	44.05 dB
HL temperature	298 K
ACL temperature	63 K

4.1.2.4. ETC Performance

As explained in section 3.2, after verifying a subsystem at ambient temperature, this will be tested under its most critical extreme temperatures.

NanoSat Lab facilities of UPC Barcelona Tech, Campus Nord, have an ISO 8 Cleanroom with a TVAC (Thermal Vacuum Chamber) and an electrodynamic shaker. They are used to conduct qualification or acceptance environmental and vibration tests to ensure in one hand that a subsystem can cope with the thermal and pressure found in outer space, and on the other hand, that it will withstand the vibrations introduced by the rocket during the launch.

Figure 18: Interior of the NanoSat Lab Cleanroom

In this section the reader can find the environmental test done to the TPR using PFM with the temperatures obtained from the thermal simulation giving a margin of 5ºC for the acceptance level.

The difference between the qualification and acceptance level in the case of the environmental tests relies on the temperature margin applied during the test. In the case of qualification tests this margin is 10ºC and for the acceptance tests 5ºC as mentioned before. Note that acceptance level is more restrictive than qualification.

Focusing on the test, this requires a pressure level lower than 10^{-5} mbar in order to simulate vacuum conditions and the thermal profile is shown in Figure 19 where the hot temperature reaches the 45ºC and the cold temperature -5ºC.

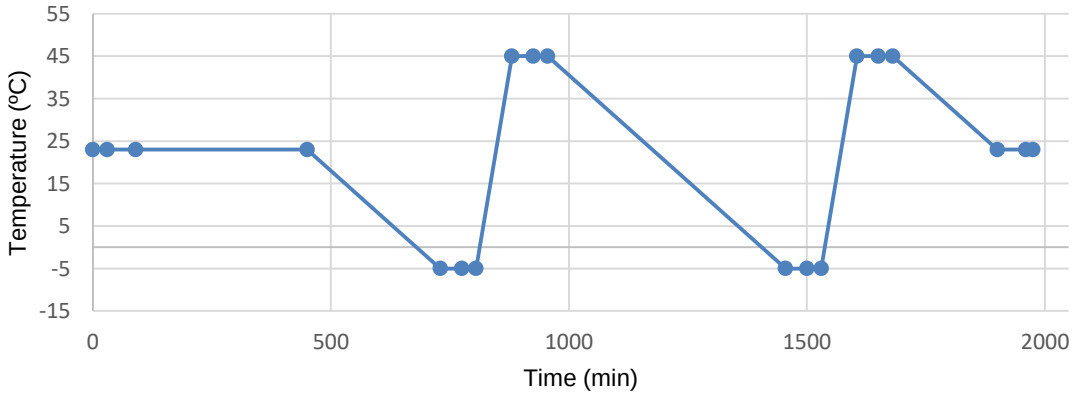

Figure 19: TPR thermal profile ETC

During the test four cycles will be performed, two hot and two cold plateaus.

Inside the TVAC there are thermocouples which monitor the temperature and, in particular, the TRP (Temperature Reference Point) thermocouple is the one used by the TVAC to decide if it is necessary to cool down or heat up the inside temperature. In Figure 20 are shown where the thermocouples were placed during the ETC.

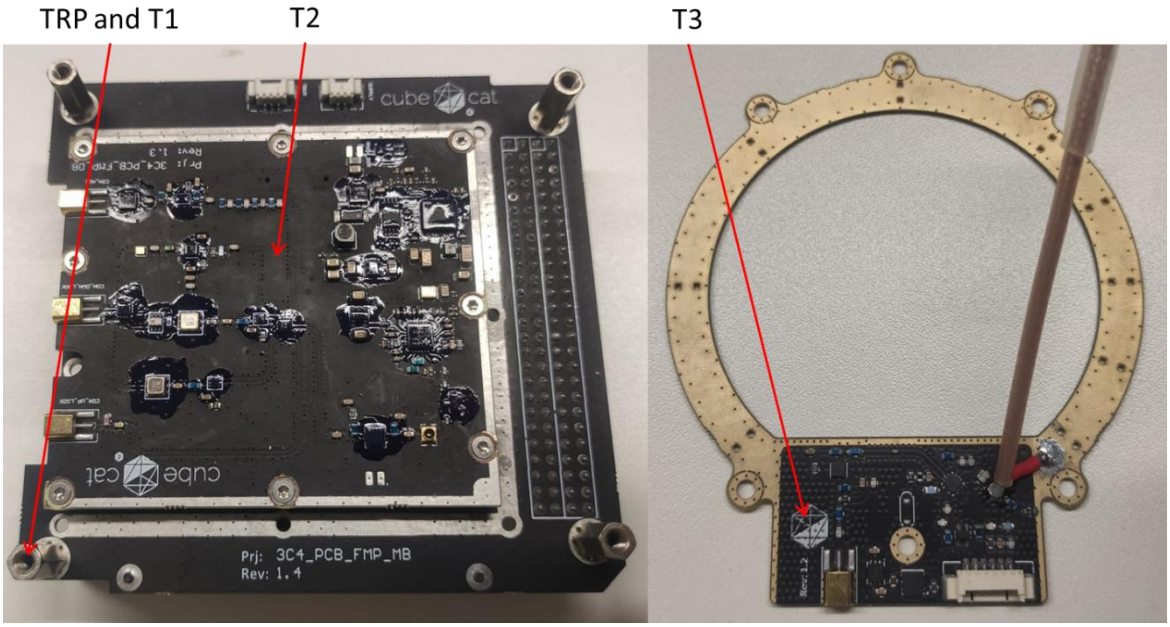

Figure 20: FMP (left) and NADS Antenna Bottom (right) thermocouples placing

Due to TVAC limitations on heating or cooling the DUT (Device Under Test), the test was performed during two days. First day was performed the two first cold and hot plateaus and during the second day the rest of two cold and hot plateau.

The temperature profile captured by PicoLog, which is the software used for plotting the temperatures read by each thermocouple from inside the TVAC, during the first day of test is shown in Figure 21. Blue trace corresponds to the TRP thermocouple, red trace to the shroud from the TVAC cooling system, and traces grey and green to the FMP and NADS Antenna Bottom respectively.

An interesting fact occurred during the test is that when gathering the data from the TPR, the FMP as well as the NADS Antenna Bottom temperature increases (Figure 21 yellow circles). This is because during the test, most of the components radiate heating the PCBs' temperature.

After the temperature profile graph there are other graphs that collects the power gathered during each hot and cold plateau from the TPR at its pass band (Figure 22 and Figure 23). Moreover, by its side it is added a graph with the corresponding temperature calculated in the same way done in the calibration loads validation by using equation (9).

Analysing the data obtained, it can be seen that the power collected during the hot plateau it is 2-3 dB higher than during the cold plateau. The reason why this happens is because an amplifier it is characterized by its two-port S-parameters (S_{ij}), and its three noise parameters: noise resistance (R_n), optimum input complex reflection coefficient (Γ_{opt}) and minimum noise factor (F). Those three noise parameters as well as the S- parameters, a part of being frequency dependant, they are temperature dependant meaning that at different temperatures, their value may vary and that is why the power values are slightly different between the hot and cold plateaus since the ACL is characterized by a LNA [11].

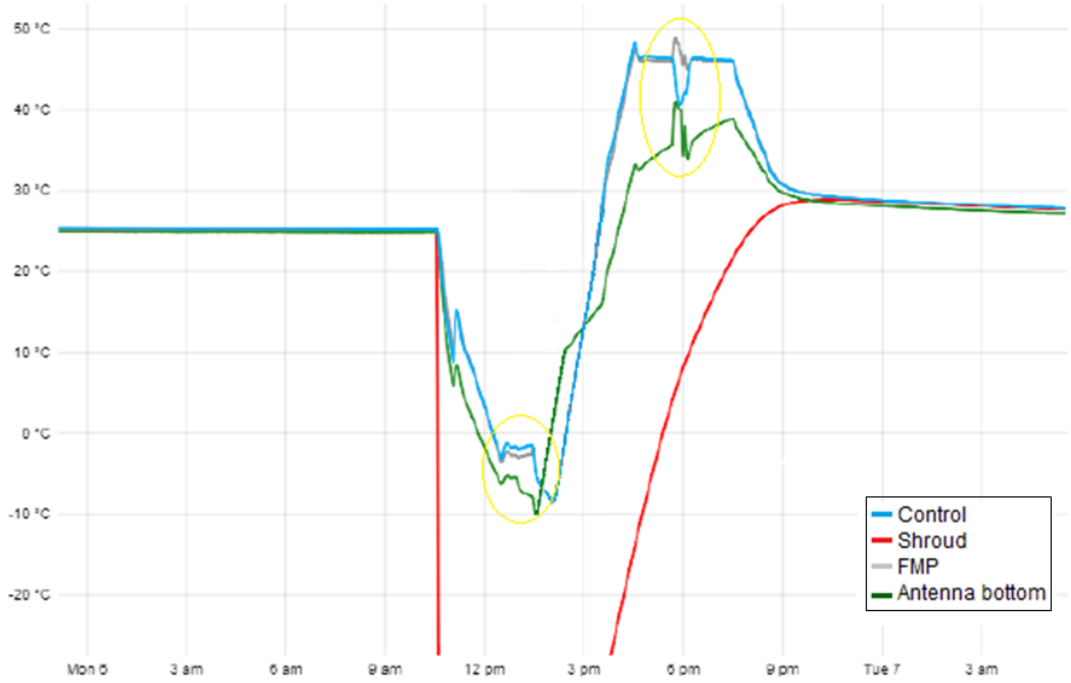

Figure 21: First day ETC temperature profile

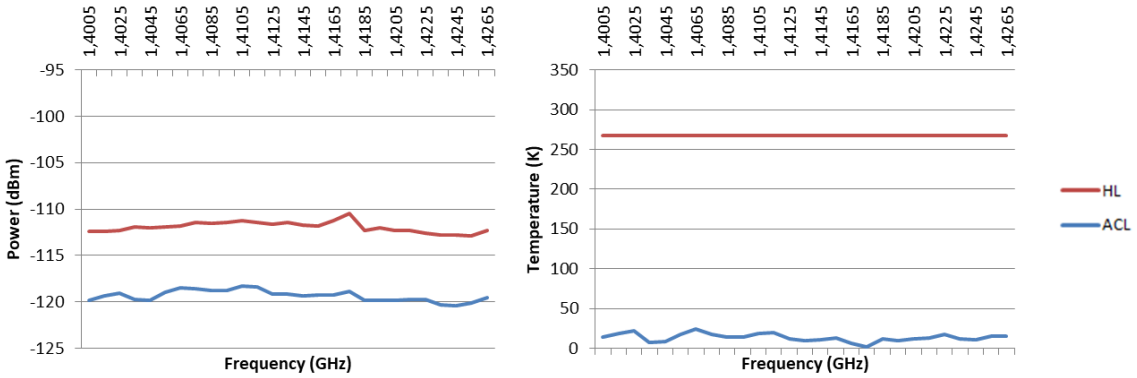

Figure 22: Data gathered during first cold plateau

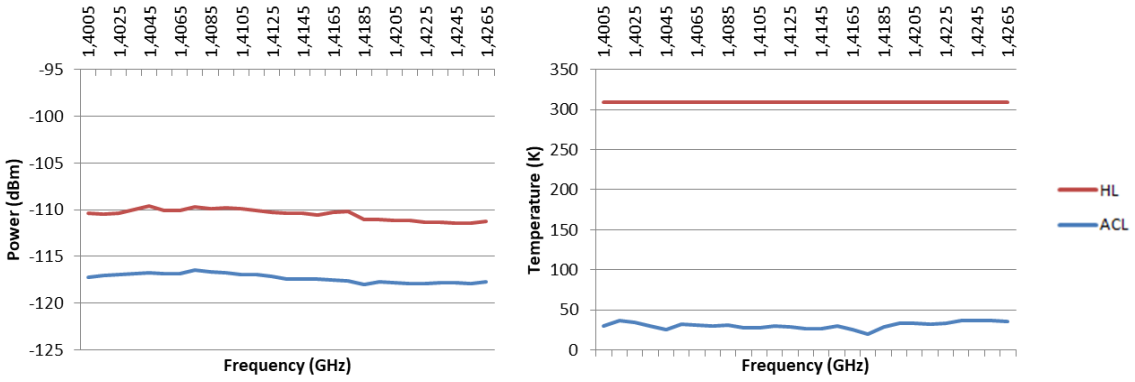

Figure 23: Data gathered during first hot plateau

Regarding to the second day of test, the temperature profile captured by PicoLog is shown in Figure 24 and the power and temperature gathered during the cold and hot plateaus in Figure 25 and Figure 26 respectively. Note that during the test, the temperature of the PCBs increased as it happened during the first day of test campaign (Figure 24 yellow circles).

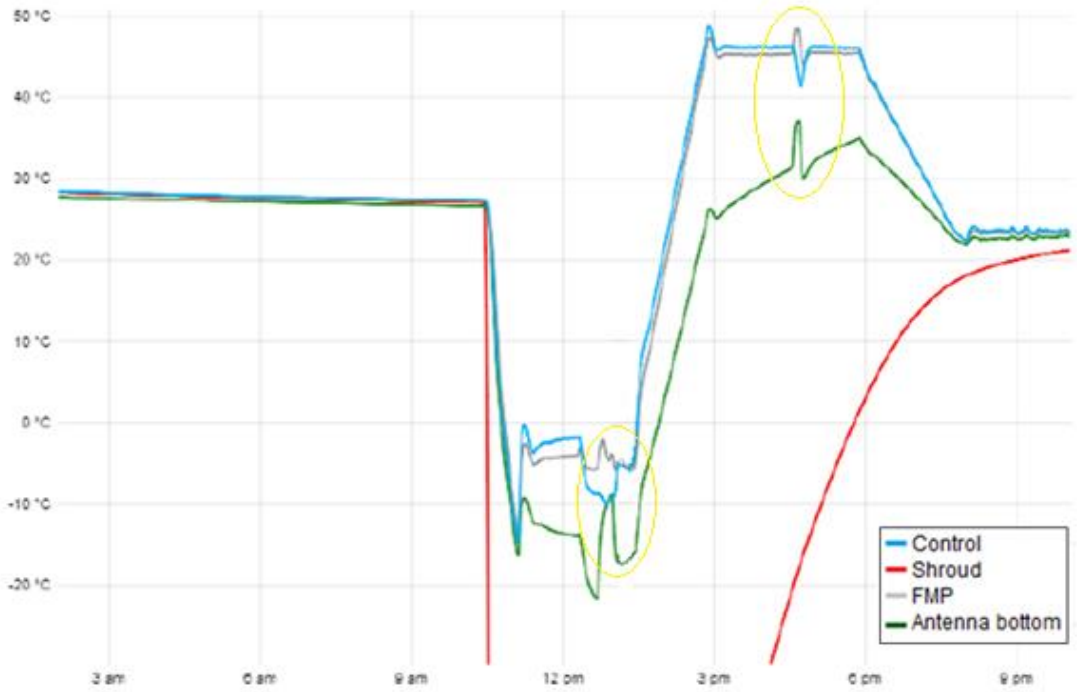

Figure 24: Second day ETC temperature profile

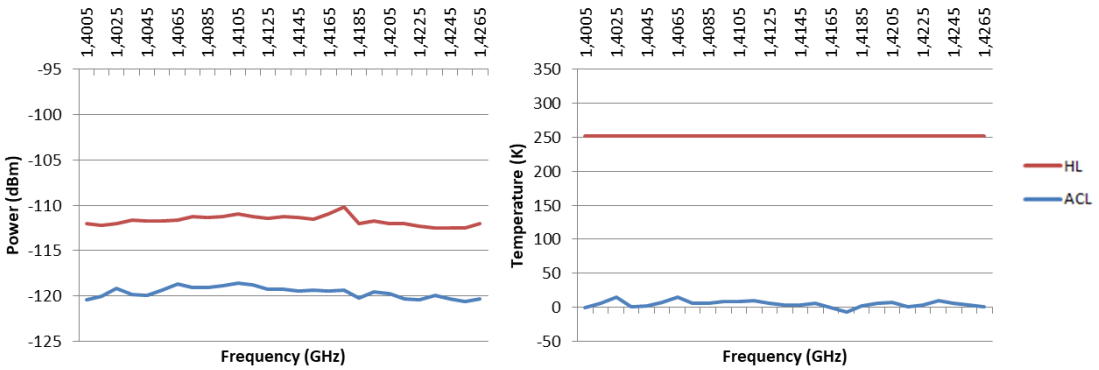

Figure 25: Data gathered during second cold plateau

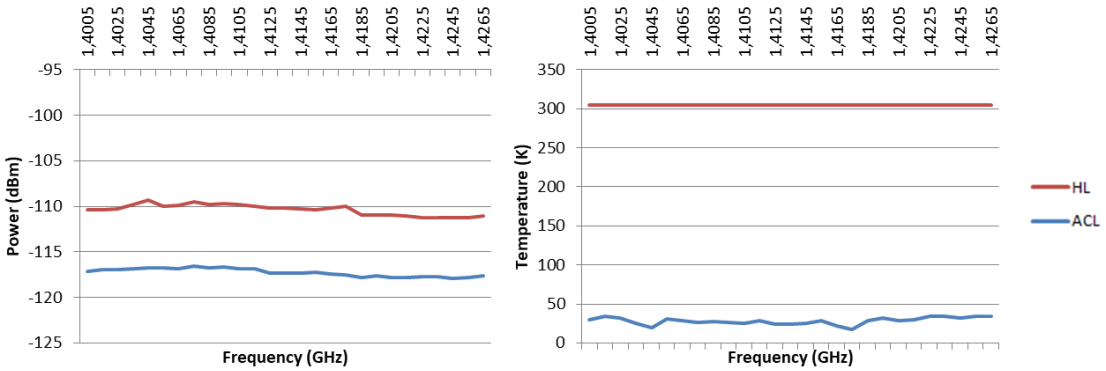

Figure 26: Data gathered during second hot plateau

Comparing the results obtained from both days of test, during cold plateaus, there are not significant differences between the collected powers, and similarly with the temperatures. Power is close to $P_{HL} = -112$ dBm for the HL and for the ACL close to $P_{ACL} = -120$ dBm. This is translated into a T_{cold} between 0 and 25 K.

The same occurs when comparing the results during the hot plateaus that the power for the HL is close to $P_{HL} = -110$ dBm and for the ACL close to $P_{ACL} = -117$ dBm. This is translated into a T_{cold} closer to the 25 K.

Thanks to the fact that there are not practically difference between the data collected in a specific temperature and the stabilization of its values in the whole pass band, the TPR performance at its extreme temperatures simulated works properly.

Table 3: Payload traceability matrix

	Val. 1	Val. 2	Val. 3	Val. 4	Val. 5	Val. 6
Req. 1	✓					
Req. 2		✓				
Req. 3			✓			
Req. 4				✓		
Req. 5					✓	
Req. 6						✓

4.2. COMMS Verification

COMMS subsystem is the responsible to provide the mechanism to the satellite for its communication with the GS once in orbit by retrieving Telemetry, Tracking & Command (TT&C), and transmitting the beacon and scientific data. Satellites have the restriction that only are able to communicate with the GS if they are in contact. So, all the data to be transmitted must be processed and stored before this happens.

In order to not interfere with other subsystems, the frequency band used by COMMS is the UHF centred at $f_c = 437.35$ MHz [10].

In the following subsections, the reader can find the verification of the COMMS PFM subsystem and the debugging to find an anomaly related in the transmission chain.

4.2.1. Block Diagram

COMMS subsystem is located in the same PCB as AOCS even though this thesis only collects the verification performed over COMMS.

COMMS subsystem is composed of different modules formed by different hardware components as it can be seen in the block diagram Figure 27.

- µC (STM32L476) [21]: this microcontroller manages the transceiver and implements physical and link layer protocols. It has also the capability to interact with the OBC module.
- Transceiver (CC1101) [20]: it is the RF transceiver from Texas Instruments that operates at UHF.
- Transmitting chain: this module is used when a transmission from ^{3}CAT-4 towards the GS needs to be done. It is defined by a PA (power amplifier, model RF5110G) [19] and a PM (true Power Measuring system, model ADL5904) [18].
- Receiving chain: this module is used when the spacecraft receives a packet from the GS. It is defined by a 3rd order LC filter and a LNA [13].
- Switch (SKY13330-397LF) [17]: This is a SPDT (Single Pole Double Throw) switch in charge of changing the signal path between the transmitting or receiving chains.

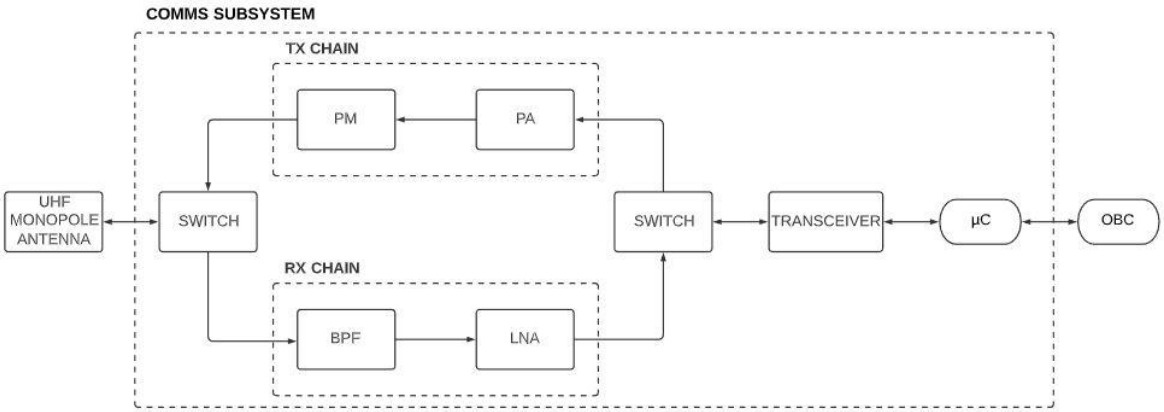

Figure 27: COMMS subsystem block diagram

4.2.2. Requirements

Table 4: COMMS requirements

Requirement	Description
Req. 1	The COMMS shall work in the UHF amateur bands via radio links.
Req. 2	The COMMS receiving chain shall have a gain larger than 15 dB.
Req. 3	The COMMS shall have a maximum Noise Figure of 5 dB in the receiving chain.
Req. 4	The COMMS shall transmit the data at a minimum power of 27 dBm.

4.2.3. Performance at Ambient Temperature

Since COMMS can be differenced whether if it is in transmitting or receiving configurations, the verification was done first focusing on the receiving chain and second focusing on the transmitting chain.

4.2.3.1. Receiving chain

The main parameters to verify when COMMS subsystem is working in reception mode, a part from checking the correct values such as the temperature read by sensors, frequency and RSSI would be the calculation of the subsystem's gain and its NF.

Table 5 summarizes the main parameters gathered by COMMS from a received packet when having a RF signal at its input of $P_{in} = -80$ dBm centred at $f_c = 437.35$ MHz simulating one possible signal received by the spacecraft from the GS.

Table 5: Parameters acquired from a reception packet

Parameter	Value
Frequency	437350016 Hz
Internal Temperature	26.3 ºC
External Temperature	27.2 ºC
$\mathrm{RSSI}_{-80dBm\_input}$	-63 dBm

The gain is obtained by subtracting the input power from the RSSI. Taken into account the losses introduced by the RF wire and the RSSI precision, the gain value will be more accurate. Therefore, knowing that the losses are $L = 0.8$ dB and that the precision is ± 1 dB, the receiver's gain results:

$$G = RSSI - (P_{in} - L) = -63\ dBm - \left(-80\ dBm - 0.8\ dB\right) = 17.8 \pm 1\ \text{dB} \quad (10)$$

Revising the receiver's LNA datasheet [13], at $f = 450$ MHz the minimum gain is 21.5 dB and its typical value is 23 dB. The obtained gain in equation (10) is 3.7 dB below the minimum value but this is due to that the central frequency is slightly shifted.

On the other hand, the last important parameter to obtain is the receiver's NF. This one is limited by a requirement that says that the noise figure for the receiver chain must be lower than 5 dB.

Proceeding in the same way done when validating the NF from the TPR, it can be defined the system of equations (11).

$$\begin{cases} N[dBm] = 10log_{10}(Gk(T_A + T_R)B) + 30dBm, \\ NF = 10log_{10}\left(1 + \frac{T_R}{T_0}\right). \end{cases} \quad (11)$$

In this case, noise power results the value of RSSI when there is not input signal but a ML which is $N = RSSI_{ML\_input} = -106$ dBm. On the other hand, the bandwidth set for the reception mode is $B = 58$ kHz and the antenna's temperature it is as well the environmental temperature during the test since a ML it is placed at its input. This means that $T_A = 25$ºC $= 298$ K.

Once all the parameters known are defined, solving the system of equation (11), T_R and NF results:

$$T_R = 10^{\frac{N-G-30}{10}} \cdot \frac{1}{kB} - T_A = 10^{\frac{-106-17.8-30}{10}} \cdot \frac{1}{1.38 \cdot 10^{-23} \cdot 58 \cdot 10^3} - 298 = 222.8 \text{ K}$$

$$NF = 10log_{10}\left(1 + \frac{T_R}{T_0}\right) = 10log_{10}\left(1 + \frac{222.8}{290}\right) = 2.48 \text{ dB}$$

Taking into account the RSSI precision of ± 1 dB and calculating again the noise figure, the minimum results $NF_{min} = 1.46$ dB and the maximum $NF_{max} = 3.49$ dB. However, the requirement is always fulfilled including for the worst case.

After the analysis, Table 5 can be extended including all the parameters that define the reception chain from COMMS subsystem resulting:

Table 6: COMMS Rx chain main parameters

Parameter	Value
Frequency	437350016 Hz
Internal Temperature	26.3 ºC
External Temperature	27.2 ºC
$\text{RSSI}_{-80dBm\_input}$	-63 dBm
Current consumption	127 mA
Gain	17.8 dB
Noise Figure	2.48 dB

4.2.3.2. Transmitting chain

The parameter to verify when COMMS subsystem is working in transmitting mode is mainly the transmitted power.

The transmitting chain is composed by a PA and a PM. The PA provides a fixed power at its output when having a minimum input power. According to the datasheet of this component, when the PA is powered by a supply voltage of 3.3 V and the RF signal power at its input is between +4.5 and +9.5 dBm (typically 7 dBm), the output RF signal power should be higher than +30 dBm. The value of the input power is controlled by the transceiver (CC1101).

The PM monitors the transmitted signal after the PA of the subsystem allowing the µC to read this power value using an analog pin of this integrated circuit.

In order to check the output power from the transmission chain, this one was connected to the spectrum analyzer. An important aspect to take into account when performing this test is that a power level of +30 dBm (this is 1 Watt) it is too much for the spectrum analyzer, since the typical RF signal power oscillates from -120 dBm to -60 dBm, and it could cause irreversible damages to the spectrum analyzer if attenuators are not used between COMMS' output and this one.

The first performance captured from the transmission chain with the spectrum analyzer is shown in Figure 28.

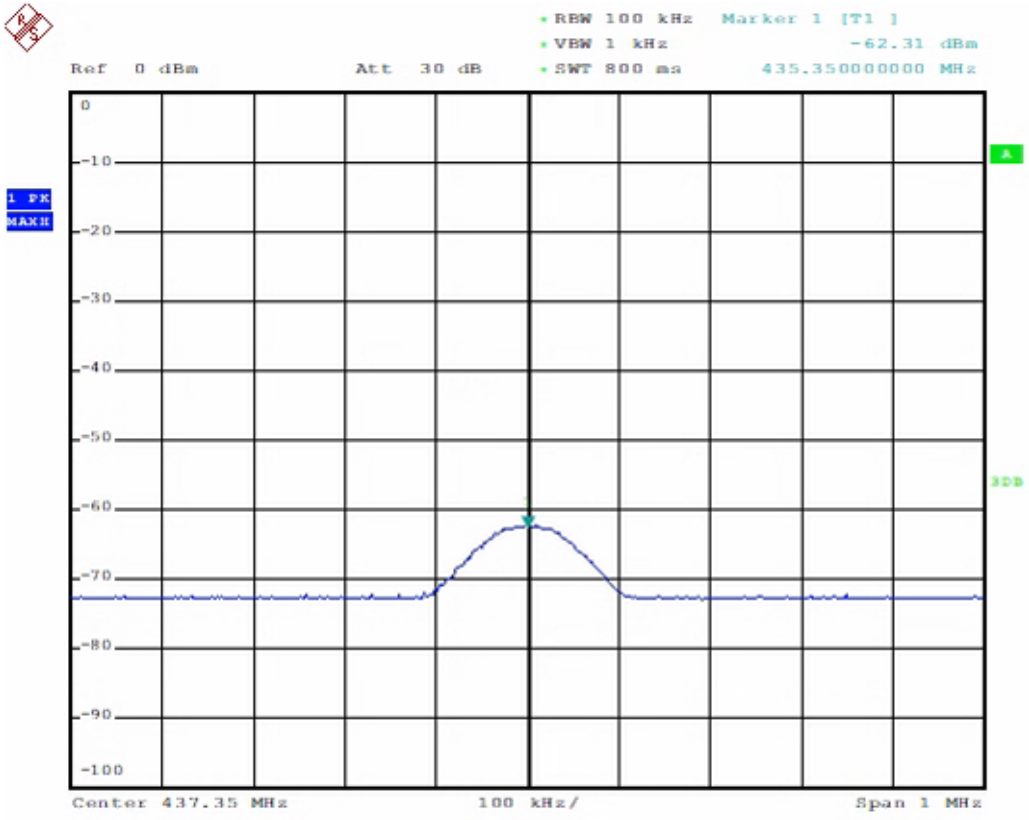

Figure 28: COMMS transmission chain output

Knowing that between the COMMS' output and the spectrum analyzer were placed 3 RF attenuators of 30 dB each and furthermore that the losses introduced by the RF wire were $L = 0.8$ dB, the transmitted power results:

$$P_{TX} = P_{RX} + Attenuators + L = -62.31dBm + 90dB + 0.8dB = 28.49 \text{ dBm}. \quad (12)$$

At this point it was realized that something wrong was happening in the transmission chain because the transmission power were lower than the minimum guaranteed by the PA manufacturer datasheet.

The first thing performed during the debugging consisted of changing the PA input power that is controlled by the transceiver to see if the transmitted power improves.

According to the transceiver's datasheet, the output power is proportional to a constant named "PATABLE" that should be between 0x84 and 0xC8 in hexadecimal to provide an output power from 5 dBm to 7 dBm. Table 7 summarizes the analysis performed to the PA for different values of the transceiver's constant. Note that the transmitted power increases with the constant set, but still it is not enough. The PA it is not working correctly in a first view because when having an input power of +7 dBm, its output power it is not higher than +30 dBm.

Table 7: PA analysis

Constant	$P_{transiver}$ [dBm]	P_{RX} [dBm]	P_{TX} [dBm]	P_{TX} [mW]	Consumption [mA]	Consumption [mW]	PA Efficiency [%]
0x84	5,0	-66,08	24,72	296,48	365	1825	16,25
0x8A	5,2	-65,88	24,92	310,46	349	1745	17,79
0x90	5,4	-66,12	24,68	293,76	335	1675	17,54
0x96	5,5	-66,38	24,42	276,69	318	1590	17,40
0x9C	5,7	-66,73	24,07	255,27	307	1535	16,63
0xA2	5,9	-65,7	25,1	323,59	370	1850	17,49
0xA8	6,1	-65,83	24,97	314,05	370	1850	16,98
0xAE	6,3	-64,88	25,92	390,84	370	1850	21,13
0xB4	6,5	-64,58	26,22	418,79	414	2070	20,23
0xBA	6,6	-63,61	27,19	523,60	414	2070	25,29
0xC0	6,7	-63,77	27,03	504,66	416	2080	24,26
0xC8	7,0	-62,31	28,49	706,32	423	2115	33,40

In order to discard that the BPF present at the PA adaptation circuit is attenuating somehow the RF signal centred at $f_c = 437.35$ MHz more than expected, the second debug consisted in a frequency shift between $f_1 = 433.35$ MHz and $f_2 = 437.35$ MHz when the transceiver constant is set at 0x90 to see its behaviour.

Figure 29 shows the spectral response when using the spectrum analyzer “max hold” function for seeing in the whole band its behaviour. Since it has the same response in the whole band, the hypothesis before can be discarded.

The last decision was to replace the PA by another one and see if the transmitted power improves, which would mean that the PA was damaged.

According to the result obtained with the new PA replaced shown in Figure 30, having the same situation of 3 attenuators of 30 dB each and losses presented by the RF wire of $L = 0.8$ dB, the power transmitted results:

$$P_{TX} = P_{RX} + Attenuators + L = -59.08\ dBm + 90\ dB + 0.8\ dB = 31.72\ \text{dBm} \quad (13)$$

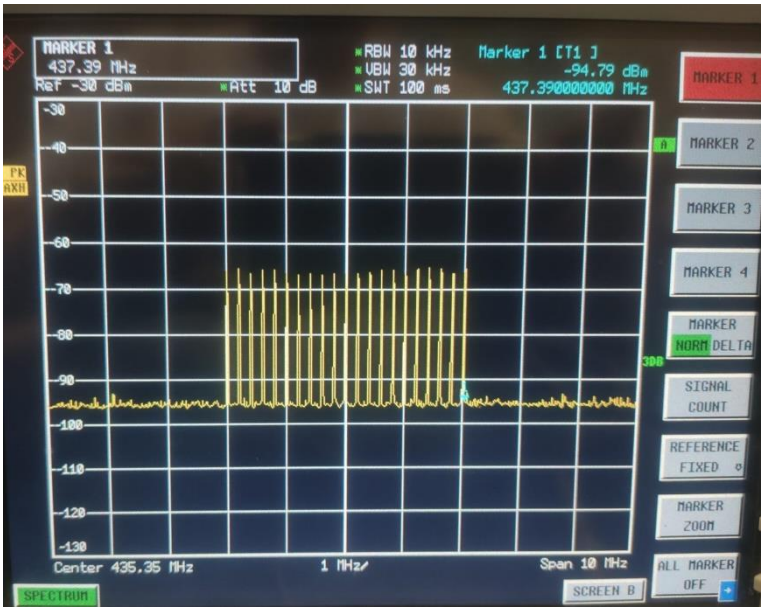

Figure 29: COMMS transmission chain frequency shift

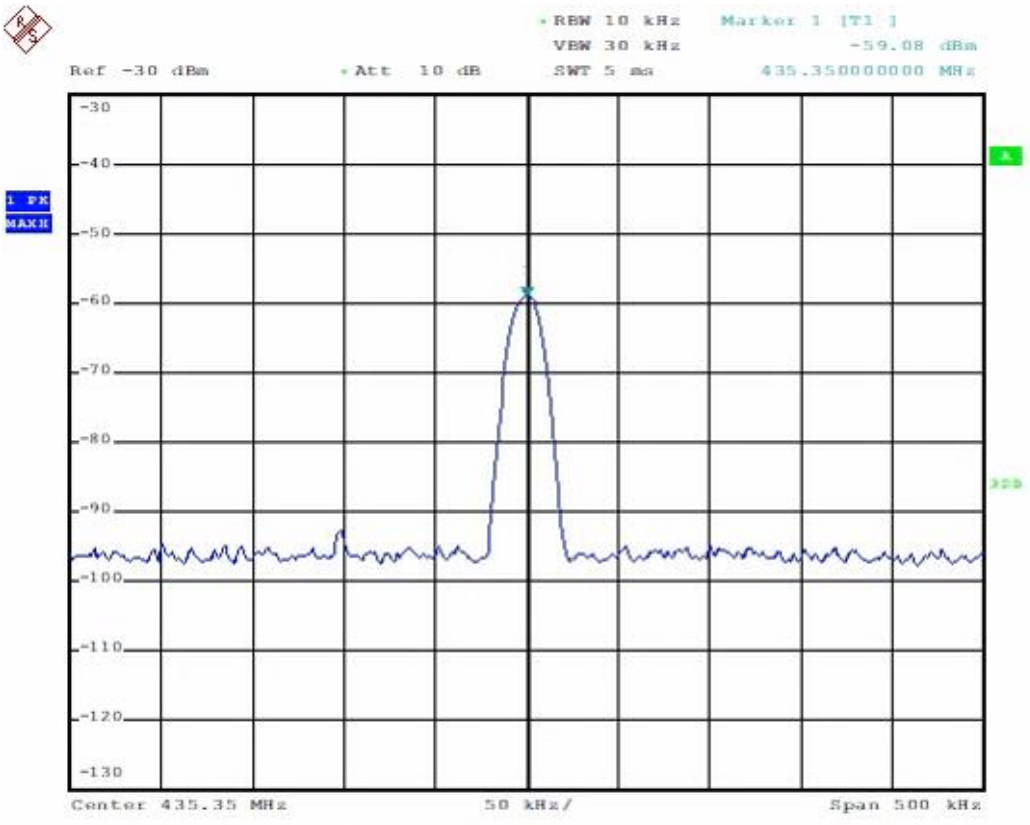

Figure 30: COMMS transmission chain output

The new PA meets the minimum transmitted power meaning that the PA used before was damaged during the manufacturing or soldering.

With this final result it concludes the COMMS verification.

Table 8: COMMS traceability matrix

	Val. 1	Val. 2	Val. 3	Val. 4
Req. 1	✓			
Req. 2		✓		
Req. 3			✓	
Req. 4				✓

5. Budget

Table 9: Money spent on components, equipment and licenses

PCBs		UNITS	COST/UNIT	COST
NADS ANTENNA BOTTOM V2.0		1	€ 81,98	€ 81,98
FMP	MOTHERBOARD	1	€ 83,96	€ 83,96
	DOUGHTERBOARD	1	€ 82,83	€ 82,83
COMMS&AOCS		1	€ 83,96	€ 83,96
COMPONENTS		**UNITS**	**COST/UNIT**	**COST**
RF COMPONENTS	SMA TO SMA	1	€ 9,31	€ 9,31
	MMCX TO MMCX	1	€ 2,61	€ 2,61
	50Ω ML	1	€ 1,60	€ 1,60
	30dB Attenuator	3	€ 16,82	€ 50,46
	MMCX TO SMA	1	€ 7,75	€ 7,75
	MS 156 PLUG-SMA PROBE	1	€ 17,78	€ 17,78
NADS ANTENNA BOTTOM V2.0	SWITCH (SKY13373-460LF)	1	€ 1,05	€ 1,05
	ACL LNA (SPF5043Z)	1	€ 3,26	€ 3,26
	LNA (SKY67150-396LF)	1	€ 5,42	€ 5,42
	3V3 LDO (LP5900)	1	€ 1,11	€ 1,11
	5V LDO (LP38693)	1	€ 1,64	€ 1,64
	RESISTORS	6	€ 0,60	€ 3,60
	CAPACITORS	19	€ 1,50	€ 28,50
	INDUCTORS	8	€ 0,25	€ 2,02
FMP	SWITCH (SKY13373-460LF)	1	€ 1,05	€ 1,05
	SAW FILTER (TA1077A)	1	€ 1,45	€ 1,45
	LNA (MAX2659ELT+)	1	€ 1,40	€ 1,40
	SWITCH (SKY13415-485LF)	1	€ 1,88	€ 1,88
	LNA (PMA-5451+)	1	€ 2,36	€ 2,36
	SDR (NooElec Nano 3)	1	€ 25,46	€ 25,46
	RESISTORS	2	€ 0,60	€ 1,20
	CAPACITORS	6	€ 1,50	€ 9,00
	INDUCTORS	5	€ 0,25	€ 1,26
COMMS	SWITCH (SKY13330-397LF)	2	€ 0,85	€ 1,70
	PM (ADL5904)	1	€ 5,49	€ 5,49
	PA (RF5110G)	1	€ 10,04	€ 10,04
	LNA (SKY67150-396LF)	1	€ 5,42	€ 5,42
	TRANSCEIVER (CC1101RGPR)	1	€ 3,66	€ 3,66
	µC (STM32L476)	1	€ 9,11	€ 9,11
	RESISTORS	8	€ 0,60	€ 4,80
	CAPACITORS	30	€ 1,50	€ 45,00
	INDUCTORS	9	€ 0,25	€ 2,27
SOFTWARE		**MONTHS**	**COST/MONTH**	**COST**
ALTIUM PCB DESIGN		6	€ 36,95	€ 221,70
SYSTEM WORKBENCH FOR STM32		6	€ -	€ -
MEGSE	**USEFUL LIFE**	**MONTHS**	**PRICE**	**DEGRADATION COST**
SPECTRUM ANALYZER DEGRADATION	25 years	4	€ 20.000,00	€ 277,78
SIGNAL GENERATOR DEGRADATION	25 years	4	€ 20.242,00	€ 281,14
POWER SUPPLY DEGRADATION	15 years	4	€ 145,20	€ 3,23
MULTIMETER DEGRADATION	2 years	4	€ 144,50	€ 24,08
			TOTAL	**€ 1.409,31**

Table 10: Salary of a junior engineer for developing this project

TASK	HOURS	COST/HOUR	COST
TPR VERIFICATION AND DEBUGGING	300	€ 8,00	€ 2.400,00
TPR ETC	100	€ 8,00	€ 800,00
COMMS VERIFICATION AND DEBUGGING	200	€ 8,00	€ 1.600,00
EXTERNAL CONSULTANTS	100	€ 35,00	€ 3.500,00
		TOTAL	**€ 8.300,00**

6. Conclusions and future developments:

The goal of this project was to verify the TPR experiment in one hand and the COMMS subsystem on the other hand.

Focusing first with the results obtained from the TPR, it has been a challenging validation since in a first way, all seemed to be correctly designed and working, but it was obvious that something wrong was happening there due to the fact that the behaviour was not the expected one.

When having a PCB of this magnitude, the first thing that comes to your mind is about checking all the integrated circuits searching for damaged or bad soldered ones, but it does not come to your mind the possibility of a capacitor lacking or the wrong value of an inductor among the other anomalies found during the debugging.

Moreover, it was not a specific anomaly the responsible of its bad behaviour, but the cumulus of all of them that caused the undesired behaviour of the TPR.

It is worth to mention that results could be improved by placing an isolator at the ACL LNA's output to improve the matching and eliminate the harmonics once the antenna or the HL are activated. But since it would be necessary a new layout design and validation, the applied solution lies in eliminating the undesired and/or wrong samples by software.

On the other hand, regarding to the ETC performed to the TPR, it has been useful a part from validating that the TPR is working without problems in the most extreme temperatures that will cope with once in orbit, to realize that the FMP is suffering some problems when accessing to the microSD of its computer where there are stored all the experiments scripts during cold temperatures. This fact was not noticed before and it could be due to the degradation of the microSD. The proposed solution consists in replacing the microSD for a new one for futures tests under cold temperatures.

By last but not least, focusing on COMMS verification and going straight to the transmission chain that was the one presenting problems, although the transmitted power was above the one predicted in the link budget which was $P_{TX} = 27$dBm, according to the PA features, this should be higher than $P_{TX} > 30$dBm. So, it was mandatory to find which was the reason of its bad performance, not only because it was losing more than half of the power, since a 2 dB loss translates into a loss of half in linear scale, but for improving the CubeSat efficiency that is once of most important and challenging aspects present in these kind of spacecraft.

Despite all the outstanding improvements done to the payload and COMMS, many others are still pending like the characterization of how gain fluctuations by calculating Allan's variance of the LNA from the TPR affects in terms of temperature. This is translated into a requirement of a thermal stability to ensure a temperature precision of the TPR.

Bibliography:

[1] UPC NanoSat Lab web page, 2020 [Online] Available: https://nanosatlab.upc.edu/en [Accessed: 13 August 2020].

[2] NASA ELaNa web page, 2020 [Online] Available: https://www.nasa.gov/mission_pages/smallsats/elana/index.html [Accessed: 13 August 2020].

[3] A. Camps. "Nanosatellites and Applications to Commercial and Scientific Missions". [Online] Available: https://www.intechopen.com/books/satellites-missions-and-technologies-for-geosciences/nanosatellites-and-applications-to-commercial-and-scientific-missions [Accessed: 13 August 2020] DOI: 10.5772/intechopen.90039

[4] W. Emery, A. Camps. " Introduction to Satellite Remote Sensing", 1st ed. 2017 ISBN: 978-0-12-809254-5

[5] M. Tiuri, "Radio astronomy receivers," in IEEE Transactions on Antennas and Propagation, vol. 12, no. 7, pp. 930-938, December 1964, doi: 10.1109/TAP.1964.1138345.

[6] Sobjaerg, Sten & Skou, Niels & Balling, Jan. (2009). "Measurements on Active Cold Loads for Radiometer Calibration." Geoscience and Remote Sensing, IEEE Transactions on. 47. 3134 - 3139. 10.1109/TGRS.2009.2017015.

[7] D'Addario, Larry R.. "Gain Stability : Requirements and Design Considerations. " 2003 [Online] Available: http://legacy.nrao.edu/alma/memos/html-memos/alma466/memo466.pdf

[8] Juan D Gallego, Isaac López-Fernández, Carmen Diez, and Alberto Barcia "Experimental results of gain fluctuations and noise in microwave low-noise cryogenic amplifiers", May 2004, doi:10.1117/12.547097

[9] R. Castellà Rubinat. "UHF Communications system for Cubesats missions". M.S. thesis, Faculty of Pompeu Fabra and Polytechnic University of Catalonia, Spain, 2018.

[10] The International Amateur Radio Union, UHF coordination, 2017 [Online] Available: http://www.amsatuk.me.uk/iaru/finished_detail.php?serialnum=588 [Accessed: 20 August 2020]

[11] SPF5043Z: 50 MHz to 4000 MHz Low-Noise Amplifier Datasheet, 2018 [Online] Available: https://www.mouser.es/datasheet/2/412/SPF5043Z_Data_Sheet-1500773.pdf

[12] SKY13373-460LF: 0.1 to 0.6 GHz SP3T Switch Datasheet, 2016 [Online] Available: https://www.mouser.es/datasheet/2/472/SKY13373_460LF_201264N-1524768.pdf

[13] SKY67150-396LF: 300 to 2200 MHz Ultra Low-Noise Amplifier Datasheet, 2017 [Online] Available: https://www.mouser.es/datasheet/2/472/SKY67150_396LF_202922I-1524656.pdf

[14] MAX2659ELT+: GPS/GNSS Low-Noise Amplifier Datasheet, 2018 [Online] Available: https://www.mouser.es/datasheet/2/256/MAX2659-1292117.pdf

[15] SKY13415-485LF: 0.1 to 3.8 GHz SP5T Antenna Switch Datasheet, 2016 [Online] Available: https://www.mouser.es/datasheet/2/472/SKY13415_485LF_201704I-1501320.pdf

[16] PMA-5451+: 0.05 to 6 GHz Ultra Low-Noise Amplifier Datasheet, 2015 [Online] Available: https://www.mouser.es/datasheet/2/1030/PMA-5451_2b-1700947.pdf

[17] SKY13330-397LF: 0.1 to 6.0 GHz SPDT Switch Datasheet, 2019 [Online] Available: https://www.mouser.es/datasheet/2/472/SKY13330_397LF_201407D-1524797.pdf

[18] ADL5904: DC to 6 GHz Detector with Envelope Threshold Detection Datasheet, 2017 [Online] Available: https://www.mouser.es/datasheet/2/609/ADL5904-1601916.pdf

[19] RF5110G: 3V General Purpose/GSM Power Amplifier Datasheet, 2019 [Online] Available: https://www.mouser.es/datasheet/2/412/RF5110G_Data_Sheet-1398162.pdf

[20] CC1101RGPR: Low-Power Sub-1 GHz RF Transceiver Datasheet, 2020 [Online] Available: https://www.ti.com/lit/ds/symlink/cc1101.pdf?HQS=TI-null-null-mousermode-df-pf-null-wwe&ts=1597340610741&ref_url=https%253A%252F%252Fwww.mouser.es%252F

[21] STM32L476: Ultra-Low-power Arm® Cortex®-M4 32-bit MCU+FPU Datasheet, 2019 [Online] Available: https://www.mouser.es/datasheet/2/389/dm00108832-1798239.pdf

[22] SDR NooElec Nano 3, 2019 [Online] Available: https://www.nooelec.com/store/nesdr-nano-three.html

[23] LP5900: 3V3 Ultra-Low-Noise LDO for RF and Analog Circuits Datasheet, 2016 [Online] Available: https://www.ti.com/lit/ds/symlink/lp5900.pdf?ts=1597341024799&ref_url=https%253A%252F%252Fwww.ti.com%252Fproduct%252FLP5900%253FHQS%253DTI-null-null-alldatasheets-df-pf-SEP-wwe%2526DCM%253Dyes%2526dclid%253DCjkKEQjwydP5BRCrhta0h46J6_IBEiQA4c2IvkSeGU-ikT7p3mYkfwrO8bGUB7Yr-W3qL-tczbBE2PXw_wcB

[24] LP38693: 5V Ultra-Low-Noise LDO for RF and Analog Circuits Datasheet, 2015 [Online] Available: https://www.ti.com/lit/ds/symlink/lp38693.pdf?ts=1597341109968&ref_url=https%253A%252F%252Fwww.ti.com%252Fproduct%252FLP38693%253FHQS%253DTI-null-null-alldatasheets-df-pf-SEP-wwe%2526DCM%253Dyes%2526dclid%253DCjkKEQjwydP5BRCrhta0h46J6_IBEiQA4c2IvjmvU5IzWBMM2iqLmYQXuYSH9cCfmRLVggX9H0gJue7w_wcB

Appendix A. Work Plan and Gantt Chart

A1. Work Packages, Tasks and Milestones

<table>
<tr><td colspan="2">Project: Assembly & Integration</td><td colspan="2">WP ref: WP1</td></tr>
<tr><td colspan="2">Major constituent: Hardware</td><td colspan="2">Sheet 1 of 3</td></tr>
<tr><td colspan="2" rowspan="2">Short description:
During the verification phase mainly, sometimes it is necessary to replace any component if it is detected that this does not work correctly or if it is necessary to do some changes in the original circuit layout.</td><td colspan="2">Planned start date: Whenever needed
Planned end date: Whenever needed</td></tr>
<tr><td colspan="2">Start event: Whenever needed
End event: Whenever needed</td></tr>
<tr><td>Internal task T1: Welds whenever needed</td><td>Deliverables: Non</td><td>Dates: --/--/--</td></tr>
</table>

<table>
<tr><td colspan="2">Project: Verification</td><td colspan="2">WP ref: WP2</td></tr>
<tr><td colspan="2">Major constituent: Hardware</td><td colspan="2">Sheet 2 of 3</td></tr>
<tr><td colspan="2">Short description:
Before the union of all the subsystems that conforms [3]CAT-4, it is needed to check that each of them works correctly and that their function is the desired one.</td><td colspan="2">Planned start date: 17/02/2020
Planned end date: 10/08/2020</td></tr>
<tr><td colspan="2">First verification is performed over the PCB named NADS Antenna Bottom where there is located the TPR together with the calibration system.
Once the NADS Antenna Bottom is verified, next step to verify will be the TPR E2E. This is NADS Antenna Bottom + FMP.
On the other side, the subsystem COMMS will be verified as well.
For each verification, a Test Specifications and Test Procedures Standalone Subsystem Validation (TSTP) and a Test Report and Test Procedures (TRTP) are required.</td><td colspan="2">Start event: 17/02/2020
End event: 10/08/2020</td></tr>
<tr><td>Internal task T1: Verify NADS Antenna Bottom

Internal task T2: Verify NADS Antenna Bottom + FMP</td><td>Deliverables: NADS Antenna Bottom TSTP
NADS</td><td>Dates: See milestones table</td></tr>
</table>

Internal task T3: Verify COMMS	Antenna Bottom TRTP NADS Antenna Bottom + FMP TSTP NADS Antenna Bottom + FMP TRTP COMMS TSTP COMMS TRTP	

Project: Environmental Testing (ETC)	WP ref: WP3	
Major constituent: Simulation	Sheet 3 of 3	
Short description: Once a subsystem is verified at ambient temperature, this is submitted into a Thermal Vacuum Chamber (TVAC) where a temperature profiles can be set in order to test any subsystem in extreme temperatures. The NADS Antenna Bottom + FMP subsystems will perform a thermal cycling in order to verify the correct performance of the TPR. For each Environmental Test, a TSTP and a TRTP are required.	Planned start date: 13/07/2020 Planned end date: 03/08/2020 Start event: 13/07/2020 End event: 03/08/2020	
Internal task T1: Adverse temperatures test of the NADS Antenna Bottom + FMP.	Deliverables: NADS Antenna Bottom + FMP ETC TSTP NADS Antenna Bottom + FMP ETC TRPT	Dates: See milestones table

Milestones

WP#	Task#	Short title	Milestone / deliverable	Date (week)
WP2	T1	NADS Antenna Bottom Verification	TSTP	15/06/2020
WP2	T1	NADS Antenna Bottom Verification	TRTP	15/06/2020
WP2	T2	NADS Antenna Bottom + FMP Verification	TSTP	15/07/2020
WP2	T2	NADS Antenna Bottom + FMP Verification	TRTP	15/07/2020
WP2	T3	COMMS Verification	TSTP	10/08/2020
WP2	T3	COMMS Verification	TRTP	10/08/2020
WP3	T1	NADS Antenna Bottom + FMP ETC	TSTP	03/08/2020
WP3	T1	NADS Antenna Bottom + FMP ETC	TRTP	03/08/2020

A2. Time Plan (Gantt chart)

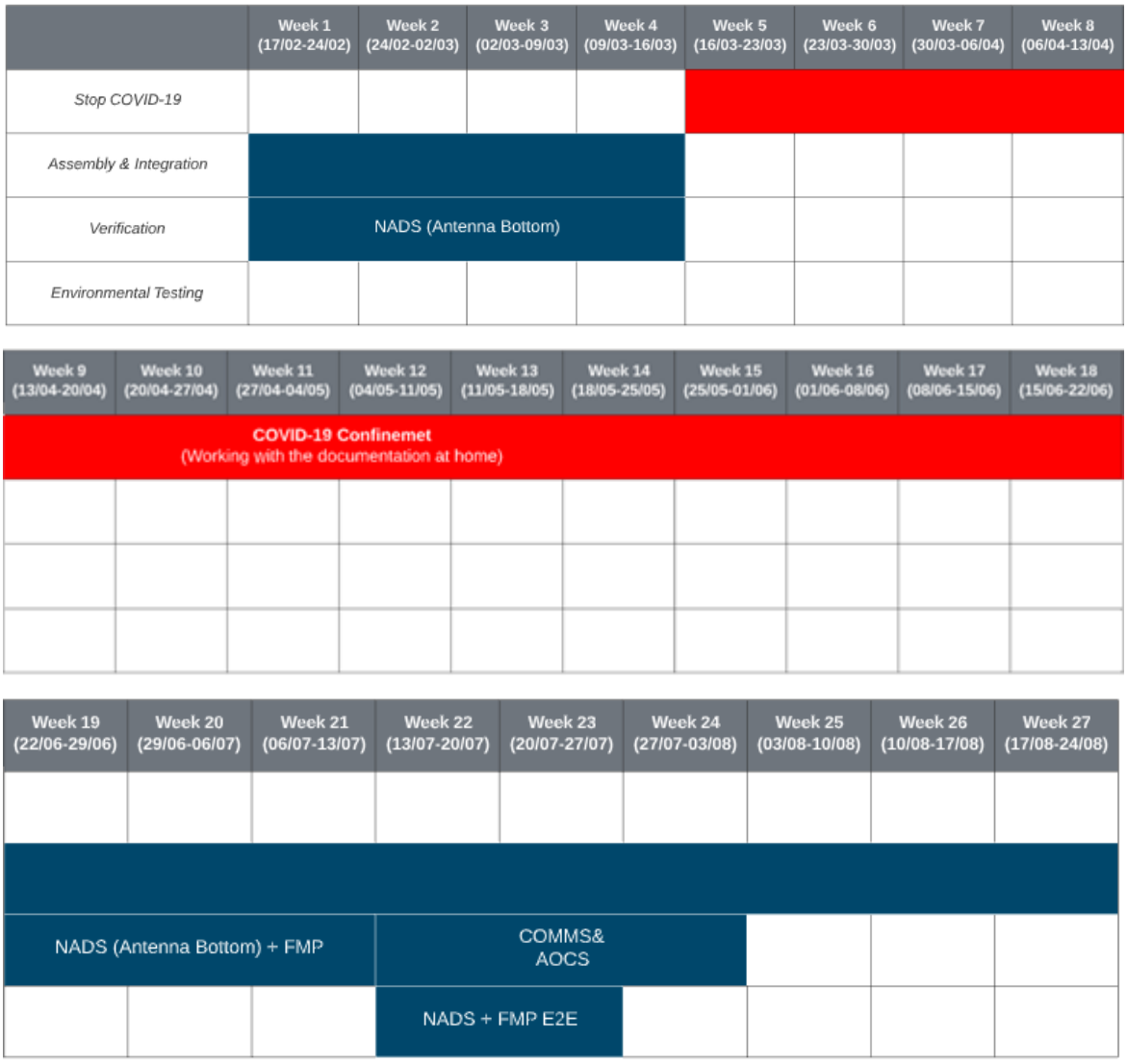

Glossary

AC	Alternating Current
ACL	Active Cold Load
AIS	Automatic Identification System
AIV	Assembly, Integration and Verification
AMP	Amplifier
AOCS	Altitude Orbit and Control Subsystem
BPF	Band Pass Filter
CDR	Critical Design Review
COMMS	Communications Subsystem
COTS	Commercial Off-The-Shelf
DUT	Device Under Test
E2E	End-to-End
EM	Engineering Model
EMI	Electromagnetic Interference
EO	Earth Observation
EPS	Electrical Power Subsystem
ETC	Environmental Test Campaign
ETSETB	Escola Tècnica Superior d'Enginyeria de Telecomunicació de Barcelona
F	Noise Factor
FFT	Fast Fourier Transform
FMP	Flexible Microwave Payload
GND	Ground
GNSS	Global Navigation Satellite System
GNSS-R	Global Navigation Satellite System - Reflectometry

GS	Ground Station
HL	Hot Load
IB	Interface Board
LDO	Low-Dropout Voltage
LEO	Low Earth Orbit
LNA	Low-Noise Amplifier
MEGSE	Mechanical Ground Support Equipment
ML	Matched Load
NADS	Nadir Antenna and Deployment Subsystem
NASA	National Aeronautics and Space Administration
NF	Noise Figure
OBC	On-Board Computer
PA	Power Amplifier
PC	Personal Computer
PCB	Printed Circuit Board
PFM	Protoflight Model
PM	Power Meter
QM	Qualification Model
R&D	Research and Development
RF	Radio Frequency
RSSI	Received Signal Strength Indicator
SAW	Surface Acoustic Wave
SDR	Software Defined Radio
SP	Solar Panels
SSV	Subsystem Standalone Verification
TPR	Total Power Radiometer

TRP	Temperature Reference Point
TVAC	Thermal Vacuum Chamber
UHF	Ultra High Frequency
UPC	Universitat Politècnica de Catalunya
VHF	Very High Frequency
VIA	Vertical Interconnect Access
ZADS	Zenith Antenna and Deployment Subsystem
µC	Microcontroller Unit